BIOCHEMISTRY
including biophysical chemistry & molecular biology

Article

pubs.acs.org/biochemistry

Light Activation of *Staphylococcus aureus* Toxin YoeB$_{Sa1}$ Reveals Guanosine-Specific Endoribonuclease Activity

Amy S. Larson and Paul J. Hergenrother*

Department of Chemistry, University of Illinois at Urbana-Champaign, Urbana, Illinois 61801, United States

Supporting Information

ABSTRACT: The *Staphylococcus aureus* chromosome harbors two homologues of the YefM-YoeB toxin−antitoxin (TA) system. The toxins YoeB$_{Sa1}$ and YoeB$_{Sa2}$ possess ribosome-dependent ribonuclease (RNase) activity in *Escherichia coli*. This activity is similar to that of the *E. coli* toxin YoeB$_{Ec}$, an enzyme that, in addition to ribosome-dependent RNase activity, possesses ribosome-independent RNase activity *in vitro*. To investigate whether YoeB$_{Sa1}$ is also a ribosome-independent RNase, we expressed YoeB$_{Sa1}$ using a novel strategy and characterized its *in vitro* RNase activity, sequence specificity, and kinetics. Y88 of YoeB$_{Sa1}$ was critical for *in vitro* activity and cell culture toxicity. This residue was mutated to *o*-nitrobenzyl tyrosine (ONBY) via unnatural amino acid mutagenesis. YoeB$_{Sa1}$-Y88ONBY could be expressed in the absence of the antitoxin YefM$_{Sa1}$ in *E. coli*. Photocaged YoeB$_{Sa1}$-Y88ONBY displayed UV light-dependent RNase activity toward free mRNA *in vitro*. The *in vitro* ribosome-independent RNase activity of YoeB$_{Sa1}$-Y88ONBY, YoeB$_{Sa1}$-Y88F, and YoeB$_{Sa1}$-Y88TAG was significantly reduced or abolished. In contrast to YoeB$_{Ec}$, which cleaves RNA at both adenosine and guanosine with a preference for adenosine, YoeB$_{Sa1}$ cleaved mRNA specifically at guanosine. Using this information, a fluorometric assay was developed and used to determine the kinetic parameters for ribosome-independent RNA cleavage by YoeB$_{Sa1}$.

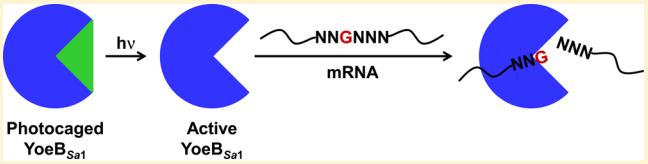

Toxin−antitoxin (TA) systems are genetic modules that are found in almost all free-living prokaryotes.[1] TA loci encode a protein toxin and a protein or RNA antitoxin and are grouped into five types on the basis of the mechanism by which the antitoxin counteracts the activity of the toxin.[2−4] In Type II TA systems, the antitoxin is a protein that binds to the toxin and prevents it from interacting with its cellular target. The activity of Type II toxins is regulated by the differential susceptibility of the toxin and the antitoxin to proteolysis. The antitoxin is more labile than the toxin and must be continuously expressed to maintain cellular levels capable of inhibiting the toxin. Toxin inhibition is relieved by the activity of cellular proteases, which degrade the labile antitoxin and shift the antitoxin:toxin ratio to favor the free toxin, which can then act on its cellular target.[5] The targets of TA system toxins include DNA replication, protein translation, and cell wall biosynthesis. Many toxins are ribonucleases (RNases) that inhibit translation by cleaving RNA in a ribosome-dependent or -independent fashion.[2]

TA systems were originally discovered on plasmids, where they function as a postsegregational killing mechanism to maintain a plasmid in a bacterial population. If a daughter cell inherits a plasmid containing a TA locus during replication, both the antitoxin and the toxin will be expressed to form a stable, innocuous complex, and the cell will survive. However, if the plasmid is not inherited, rapid proteolytic degradation of the antitoxin will release the toxin to act on its cellular target and kill the cell, thereby eliminating plasmid-free cells from the population.[6] TA systems were subsequently discovered on the chromosomes of many bacteria and archaea.[1,7] The function of chromosomally encoded TA systems is somewhat controversial, with at least 13 proposed roles, including junk DNA, selfish genes, stabilization of mobile genetic elements, anti-addiction elements, gene regulation, growth control/stress response, persistence, growth arrest, programmed cell death, phage defense, biofilm formation, virulence, and phenotypic bistability.[8,9] However, it is generally accepted that cellular stress modulates transcription at the TA locus and stimulates degradation of the antitoxin, releasing the toxin to act on its cellular target and arrest growth until conditions become more favorable.[5] Upon the cessation of stress, the antitoxin is replenished, inactivating the toxin and allowing the cell to resume normal growth.[10] The growth arrest and eventual cell death resulting from toxin overexpression have led to the proposal that artificial toxin activation could provide an effective antibacterial strategy.[11−14]

The Gram-positive pathogen *Staphylococcus aureus* is the leading cause of bloodstream, lower respiratory tract, and skin and soft tissue infections worldwide.[15] A recent comparative genomic analysis identified between one and seven Type II TA loci in the sequenced genomes of 14 *S. aureus* strains, including YefM-YoeB$_{Sa1}$ and YefM-YoeB$_{Sa2}$ (previously identified as Axe1-Txe1 and Axe2-Txe2, respectively)[16,17] that are homologues of the YefM-YoeB$_{Ec}$ TA system from *Escherichia coli*.[18] The toxin YoeB$_{Ec}$ possesses ribosome-independent RNase

Received: June 22, 2013
Revised: November 26, 2013
Published: November 26, 2013

activity *in vitro* as well as ribosome-dependent RNase activity *in vitro* and in cells.[19,20] $YoeB_{Ec}$ binds in the A site of the 50S ribosomal subunit, causing cleavage of mRNA transcripts three bases downstream of the start codon.[20] It is unknown whether $YoeB_{Ec}$-mediated mRNA cleavage on the ribosome results from direct catalysis by $YoeB_{Ec}$, from enhancement of the latent ribonucleolytic activity of the ribosome upon binding of $YoeB_{Ec}$, or from some combination of the two.[20]

A significant challenge when studying toxic proteins is the difficulty associated with their expression and purification in *E. coli*. Herein, we present a novel solution to this problem by incorporating a noncanonical amino acid, a photocaged tyrosine derivative, to replace a tyrosine that is critical for the activity and toxicity of $YoeB_{Sa1}$. Using protein produced through this method, the substrate specificity of $YoeB_{Sa1}$ was unveiled, allowing the creation of a fluorogenic substrate that can be used to monitor $YoeB_{Sa1}$ activity.

EXPERIMENTAL PROCEDURES

Bacterial Strains. MRSA clinical isolates were from a previously published collection.[21] *E. coli* DH5α and NiCo21(DE3) were used for cloning and protein expression, respectively.

Primers. All primers used for polymerase chain reaction (PCR), reverse transcription PCR (RT-PCR), cloning, and site-directed mutagenesis were synthesized by Integrated DNA Technologies (IDT) and are listed in Table S1 of the Supporting Information.

PCR Analysis of Clinical Isolates. Total DNA was previously purified from a diverse collection of 78 clinical isolates of MRSA.[21] Primers YefM-$YoeB_{Sa1}$-F and YefM-$YoeB_{Sa1}$-R or YefM-$YoeB_{Sa2}$-F and YefM-$YoeB_{Sa2}$-R were used to amplify the *yefM-yoeB*$_{Sa1}$ or *yefM-yoeB*$_{Sa2}$ loci, respectively, from the total DNA. Primers $YefM_{Sa1}$-NdeI-F, $YefM_{Sa1}$-XhoI-R, $YoeB_{Sa1}$-NdeI-F, $YoeB_{Sa1}$-HindIII-R, $YefM_{Sa2}$-NdeI-F, $YefM_{Sa2}$-HindIII-R, $YoeB_{Sa2}$-NdeI-F, and $YoeB_{Sa2}$-HindIII-R were used to amplify the *yefM*$_{Sa1}$, *yoeB*$_{Sa1}$, *yefM-yoeB*$_{Sa1}$, *yefM*$_{Sa2}$, *yoeB*$_{Sa2}$, and *yefM-yoeB*$_{Sa2}$ operons from the total DNA of strains NRS27 and NRS76. PCR amplification was performed on a DNA thermocycler using previously described reaction conditions.[21,22] PCR products were separated by electrophoresis on 1% agarose gels and stained with ethidium bromide.

Sequencing Analysis. Approximately 10% of the PCR products generated via PCR amplification of the *yefM-yoeB*$_{Sa1}$ and *yefM-yoeB*$_{Sa2}$ loci were sequenced by the University of Illinois W. M. Keck Center for Comparative and Functional Genomics. Sequence data were analyzed using BioEdit version 7.0.5.3. The sequences were aligned using CLUSTAL W[23] and used as query sequences to search the BLAST database to verify the identity of the PCR products and homology to known genes.[24]

RT-PCR Analysis of Clinical Isolates. MRSA isolates were streaked from glycerol stocks on Brain Heart Infusion (BHI) agar. Single colonies from freshly streaked plates were inoculated into 10 mL of BHI medium and incubated aerobically at 37 °C with shaking at 250 rpm overnight (14−16 h). Overnight cultures were diluted 1:100 in 10 mL of BHI medium and incubated aerobically at 37 °C with shaking at 250 rpm until the A_{600} reached 0.6−1.0. Logarithmically growing cultures were harvested by centrifugation at 3220*g* for 10 min at 4 °C. Total RNA was purified using the FastRNA Pro Blue Kit (Qbiogene) according to the manufacturer's instructions with the modification that lysis was performed by vortexing resuspended cells at maximal speed for 5 × 1 min pulses at room temperature with recovery for 1−5 min on ice between pulses. Isolated RNA was treated with DNase I and purified with reagents from the Total RNA Kit I (Omega Bio-Tek) according to the RNA Cleanup protocol from the RNeasy Mini Handbook (Qiagen). Purified total RNA (10 ng) was used in RT-PCR and in PCR with Platinum Taq DNA Polymerase (Invitrogen) to detect DNA contamination. RT-PCR was performed with primers YefM-$YoeB_{Sa1}$-F and YefM-$YoeB_{Sa1}$-R or YefM-$YoeB_{Sa2}$-F and YefM-$YoeB_{Sa2}$-R using the Superscript III One-Step RT-PCR System with Platinum Taq (Invitrogen) as previously reported[22] with the following modifications: the annealing temperature was increased to 55 °C, and the number of cycles was reduced to 35. PCR products were separated by electrophoresis on 1% agarose gels and stained with ethidium bromide.

Construction of Plasmids. The *yoeB*$_{Sa1}$ open reading frame (ORF) was amplified via PCR from the total DNA of MRSA S4[21] with primers $YoeB_{Sa1}$-NdeI-F and $YoeB_{Sa1}$-Y88F-HindIII-R or $YoeB_{Sa1}$-Y88TAG-HindIII-R and cloned into the corresponding sites of pET-28a (Novagen) to create pET-28a-*yoeB*$_{Sa1}$-*Y88F* and pET-28a-*yoeB*$_{Sa1}$-*Y88TAG*, respectively. The *yefM-yoeB*$_{Sa1}$ ORF was amplified via PCR from the total DNA of MRSA S4[21] with primers $YefM_{Sa1}$-NdeI-F and $YoeB_{Sa1}$-HindIII-R and cloned into the corresponding sites of pET-28a. Because a single nonsilent point mutation was found in the sequence for $YefM_{Sa1}$, Quikchange site-directed mutagenesis was performed with primers $YefM_{Sa1}$-QC-F and $YefM_{Sa1}$-QC-R to create pET-28a-*yefM-yoeB*$_{Sa1}$. Site-directed mutagenesis was carried out with the Quikchange site-directed mutagenesis kit (Stratagene) according to the manufacturer's instructions with the modification that *E. coli* DH5α was used as the host strain. The *yefM*$_{Sa1}$ ORF was amplified via PCR from the total DNA of MRSA NRS3 (Network on Antimicrobial Resistance in *S. aureus*) with primers $YefM_{Sa1}$-NdeI-F and $YefM_{Sa1}$-XhoI-R and cloned into the corresponding sites of pET-28a to create pET-28a-*yefM*$_{Sa1}$. All clones were confirmed by sequencing. The following antibiotic concentrations were used: 50 μg/mL kanamycin (pET-28a), 35 μg/mL chloramphenicol (pEVOL-ONBY), and 100 μg/mL ampicillin (Pentaprobes).

ONBY Synthesis. *o*-Nitrobenzyl tyrosine (ONBY) was synthesized according to a previously published method[25] with some modifications. Two grams (11 mmol) of L-tyrosine was stirred with 1.9 g (7.6 mmol) of $CuSO_4 \cdot 5H_2O$ in 20 mL of 1 M NaOH at 60 °C for 20 min. The reaction was cooled to room temperature, quenched with hydrochloric acid, filtered, and washed with water. The resulting solid was stirred with 1.5 g (11 mmol) of K_2CO_3 and 1.8 g (8.3 mmol) of *o*-nitrobenzyl bromide in 60 mL of 75% aqueous dimethylformamide (DMF) at room temperature in the dark for 3 days. The resulting solid was filtered; washed with 75% aqueous DMF, water, 75% aqueous acetone, and ice-cold acetone; stirred in 100 mL of 1 M HCl for 2 h; filtered; stirred in 100 mL of 1 M HCl for 1 h; filtered; and washed with water and acetone. The overall yield was 1.8 g (5.7 mmol, 69%).

Purification of $YoeB_{Sa1}$-Y88F and $YoeB_{Sa1}$-Y88TAG. pET-28a-*yoeB*$_{Sa1}$-*Y88F* or pET-28a-*yoeB*$_{Sa1}$-*Y88TAG* was introduced into *E. coli* NiCo21(DE3). A single colony from a freshly streaked plate was inoculated into LB medium supplemented with kanamycin and grown at 37 °C with shaking at 250 rpm overnight (14−16 h). The overnight culture was diluted 1:100 and grown at 37 °C with shaking at 250 rpm until the A_{600}

dx.doi.org/10.1021/bi4008098 | *Biochemistry* 2014, 53, 188−201

reached 0.4−0.6. Protein expression was induced with 1 mM IPTG at 37 °C with shaking at 250 rpm for 4 h. The culture was harvested by centrifugation at 6000*g* for 5 min at 4 °C. Cell pellets were frozen at −20 °C, thawed on ice for 30 min, and resuspended in 10 mL of cold lysis buffer [20 mM Tris, 500 mM NaCl, and 60 mM imidazole (pH 7.9)]. Cells were lysed by sonication on ice at 40% amplitude for 5 min with a 1 s pulse. The lysate was cleared by centrifugation at 35000*g* for 30 min at 4 °C. The supernatant was batch-loaded onto 1 mL of 1:1 Ni-NTA agarose (Qiagen) at 4 °C for 30 min with inversion. The resin was washed with 20 mL of cold lysis buffer and eluted with 10 mL of cold elution buffer A [50 mM Tris, 500 mM NaCl, 500 mM imidazole, 1 mM TCEP, and 10% glycerol (pH 7.9)]. The eluted fraction was concentrated to ∼0.5 mL using an Ultra-15 Centrifugal Filter Unit with an Ultracel-3 membrane (Amicon), 0.2 μm filtered, and further purified on a HiLoad 16/60 Superdex 75 PG column (GE Healthcare) using fast performance liquid chromatography (FPLC) buffer A [50 mM Tris, 200 mM NaCl, 1 mM TCEP, and 10% glycerol (pH 7.9)]. Fractions containing pure protein were pooled and concentrated to ∼0.5−1 mL. Purity was assessed by sodium dodecyl sulfate−polyacrylamide gel electrophoresis (SDS−PAGE) using 4−20% TGX Mini-PROTEAN gels (Bio-Rad). The concentration was determined by densitometry and by the bicinchoninic acid (BCA) assay (Pierce) performed according to the manufacturer's instructions, with the modification that lysozyme standards were used instead of bovine serum albumin (BSA) standards.

Purification of YoeB$_{Sa1}$-Y88ONBY. pET-28a-*yoeB$_{Sa1}$-Y88TAG* and pEVOL-ONBY were introduced into *E. coli* NiCo21(DE3). A single colony from a freshly streaked plate was inoculated into LB medium supplemented with kanamycin and chloramphenicol and grown at 37 °C with shaking at 250 rpm overnight (14−16 h). The overnight culture was diluted 1:100, 100 mM ONBY dissolved in 1 M NaOH was added to a final concentration of 1 mM, and the culture was grown at 37 °C with shaking at 250 rpm in the dark. When the A_{600} of the culture reached 0.5−0.6, arabinose was added to a final concentration of 0.2% to induce expression of ONBY-aaRS. When the A_{600} of the culture reached 1.0−1.2, IPTG was added to a final concentration of 1 mM to induce expression of YoeB$_{Sa1}$-Y88ONBY. Expression was allowed to proceed at 37 °C for 15 h. The culture was harvested, and YoeB$_{Sa1}$-Y88ONBY was purified in the dark as described above for YoeB$_{Sa1}$-Y88F and YoeB$_{Sa1}$-Y88TAG.

Purification of YefM$_{Sa1}$. pET-28a-*yefM$_{Sa1}$* was introduced into *E. coli* NiCo21(DE3), and protein expression and purification were performed as described for YoeB$_{Sa1}$-Y88F and YoeB$_{Sa1}$-Y88TAG, with the modification that YefM$_{Sa1}$ was eluted with 10 mL of cold elution buffer B [20 mM Tris, 500 mM NaCl, and 500 mM imidazole (pH 7.9)]. Gel filtration was performed twice using FPLC buffer B [20 mM Tris and 500 mM NaCl (pH 7.9)] to remove RNase contamination. Fractions corresponding to the second major peak from the first gel filtration step were pooled, concentrated, and subjected to a second gel filtration step. Fractions corresponding to the second major peak from the second gel filtration step were pooled, concentrated, and used in experiments. Purity was assessed by SDS−PAGE using 4−20% TGX Mini-PROTEAN gels (Bio-Rad). Protein concentration was determined by the BCA assay (Pierce) performed according to the manufacturer's instructions using BSA standards.

ESI-MS. Five micrograms of YefM$_{Sa1}$, YoeB$_{Sa1}$-Y88F, YoeB$_{Sa1}$-Y88TAG, or YoeB$_{Sa1}$-Y88ONBY was precipitated according to a previously published method.[26] YoeB$_{Sa1}$-Y88ONBY was exposed to 312 nm light on a UV transilluminator for 0−600 s prior to precipitation. Precipitated, air-dried protein was analyzed by electrospray ionization mass spectrometry (ESI-MS) at the University of Illinois Mass Spectrometry Laboratory.

Agarose Gel RNase Activity Assay. pET-28a-*yefM-yoeB$_{Sa1}$* was digested with XhoI (NEB) at 37 °C for 3 h. The fully linearized plasmid was extracted once with a 24.5:24.5:1 phenol/chloroform/isoamyl alcohol mixture and twice with chloroform, precipitated with 3 M NaOAc (pH 5.3) and 100% EtOH, and resuspended in nuclease-free water. One microgram of linearized plasmid was used as the template for standard RNA synthesis with the T7 High Yield RNA Synthesis Kit (NEB) according to the manufacturer's instructions. RNA was purified with reagents from Total RNA Kit I (Omega Bio-Tek) according to the RNA Cleanup protocol from the RNeasy Mini Handbook (Qiagen). RNase assays were performed according to a modified published method.[19] For the light dependence of decaging, 10 pmol of YoeB$_{Sa1}$-Y88ONBY in 50 mM Tris and 5% glycerol (pH 8.0) was exposed to UV light for 0−5 min, followed by the addition of 320 ng of *yefM-yoeB$_{Sa1}$* RNA with Human Placental RNase Inhibitor (NEB) at a final concentration of 1 unit/μL. Reactions were incubated at 37 °C for 2 h and quenched by addition of 1 μg of proteinase K (Invitrogen) and incubation at 37 °C for 15 min. Eleven microliters of RNA loading dye I (95% formamide, 18 mM EDTA, 0.025% SDS, and 0.025% bromophenol blue) was then added, and samples were incubated at 95 °C for 5 min immediately prior to electrophoresis on 1.2% agarose, 0.5× TBE [45 mM Tris-borate and 1 mM EDTA (pH 8.3)], 0.1 μg/mL ethidium bromide gels. For the inhibition of YoeB$_{Sa1}$ by YefM$_{Sa1}$, YoeB$_{Sa1}$ (10, 20, or 30 pmol) in 50 mM Tris and 5% glycerol (pH 8.0) was exposed to UV light for 3 min. YefM$_{Sa1}$ (0, 10, 20, or 30 pmol) was then added. Following incubation at 37 °C for 30 min to allow formation of the YefM-YoeB$_{Sa1}$complex, 320 ng of *yefM-yoeB$_{Sa1}$* RNA was added with Human Placental RNase Inhibitor at a final concentration of 1 unit/μL. Reactions were incubated at 37 °C for 1 h, quenched, and analyzed as described above. For the time course of YoeB$_{Sa1}$ and YefM$_{Sa1}$ RNase activity, 10 pmol of YoeB$_{Sa1}$-Y88ONBY, YoeB$_{Sa1}$-Y88F, YoeB$_{Sa1}$-Y88TAG, or YefM$_{Sa1}$ was incubated with 320 ng of *yefM-yoeB$_{Sa1}$* RNA in the presence of 1 unit/μL Human Placental RNase Inhibitor in 50 mM Tris and 5% glycerol (pH 8.0). One set of reactions containing YoeB$_{Sa1}$-Y88ONBY was exposed to UV light for 3 min prior to the addition of RNA. Reactions were incubated at 37 °C for 1−20 h, quenched, and analyzed as described above.

Polyacrylamide Gel RNase Activity Assay. Quikchange site-directed mutagenesis was performed with primers PP1QC1-F and PP1QC1-R to insert a G into Pentaprobe 1 and with primers PP1QC2-F and PP1QC2-R, PP2QC-F and PP2QC-R, PP4QC-F and PP4QC-R, PP6QC-F and PP6QC-R, PP7QC-F and PP7QC-R, PP8QC-F and PP8QC-R, PP9QC-F and PP9QC-R, PP10QC-F and PP10QC-R, and PP12QC-F and PP12QC-R (Table S1 of the Supporting Information) to introduce XbaI sites into Pentaprobes 1, 2, 4, 6−10, and 12, respectively. Site-directed mutagenesis was carried out with the Quikchange site-directed mutagenesis kit (Stratagene) according to the manufacturer's instructions, with the modification that *E. coli* DH5α was used as the host strain. Pentaprobe

plasmids were digested with XbaI (NEB) at 37 °C for 3 h. Fully linearized plasmids were purified by phenol/chloroform extraction as described above. RNA was synthesized and purified as described above. RNase assays were performed according to a modified published method.[27] One microgram of $YoeB_{Sa1}$-Y88ONBY was incubated with 1 μg of Pentaprobe RNA in 50 mM Tris (pH 8.0) for 0.5−2 h at 37 °C. Reactions were quenched by addition of 1 μg of proteinase K and incubation at 37 °C for 15 min. An equal volume of RNA loading dye II (95% formamide, 5 mM EDTA, and 0.025% bromophenol blue) was then added, and the reactions were incubated at 95 °C for 5 min to denature the RNA. The products were visualized by electrophoresis on 8% polyacrylamide TBE−urea gels [89 mM Tris-borate, 2 mM EDTA, and 8 M urea (pH 8.3)] poststained with ethidium bromide.

Matrix-Assisted Laser Desorption Ionization (MALDI) RNase Activity Assay. PP7-1, PP7-2, and PP7-3 were synthesized by Genscript. Ten micrograms of $YoeB_{Sa1}$-Y88ONBY was incubated with 2 μg of oligonucleotide for 1 or 2 h at 37 °C. Reactions were quenched by addition of 10 μg of proteinase K (Invitrogen) and incubation at 37 °C for 30 min followed by precipitation with 5 M NH_4OAc (final concentration of 2 M) and 3 volumes of 100% EtOH at −80 °C. Pellets were washed with ice-cold 70% EtOH, resuspended in 1 μL of H_2O, and analyzed by matrix-assisted laser desorption ionization mass spectrometry (MALDI-MS) at the University of Illinois Mass Spectrometry Laboratory.

High-Performance Liquid Chromatography (HPLC) RNase Activity Assay. The fluorogenic chimeric oligonucleotide substrate 5′-6-FAM-AACrArArArArGrArArAAATT-IABkFQ-3′ (6-FAM, 6-carboxyfluorescein fluorophore; IABkFQ, Iowa Black fluorophore quencher) and cleavage products 5′-6-FAM-AACrArArArArG-3′ and 5′-rArArAAATT-IABkFQ-3′ were synthesized by IDT. $YoeB_{Sa1}$ (20 μM) was incubated with oligonucleotide (30 μM) in buffer at 25 °C for 5 h. HPLC was performed using an Alliance HPLC System (e2695 Separations Module, Waters) with detection at 260 nm (2489 UV/visible Detector, Waters). The full-length oligonucleotide was separated from the cleavage products on a YMCbasic S5 column (4.6 mm × 150 mm, 5 μm, Waters) using a linear gradient from 100 mM triethylammonium acetate (TEAA) (pH 7.0) to a mixture of 50 mM TEAA and 50% acetonitrile (pH 7.0) over 25 min. Peak fractions were collected, concentrated to 5−10 μL, and analyzed by MALDI-MS at the University of Illinois Mass Spectrometry Laboratory.

Fluorometric Assay. Wells of a black 384-well plate were filled with 15 μL of 0.5−20 μM intact fluorogenic substrate or cleavage products diluted in assay buffer [200 mM sodium phosphate (pH 6.0) and 5% glycerol] and allowed to equilibrate for 30 min at room temperature. $YoeB_{Sa1}$-Y88ONBY was diluted to 10 μM in assay buffer, exposed to UV light at 312 nm for 3 min, and added to wells containing intact substrate or cleavage products to a final concentration of 5 μM. Fluorescence was measured once every minute for 100 min using a Criterion Analyst AD instrument (Molecular Devices) with 485 ± 15 nm excitation and 530 ± 15 nm emission filters and a 505 nm cutoff dichroic mirror. The fluorophore was excited with a 1000 W continuous xenon arc lamp with 10 reads per well. Three separately purified batches of $YoeB_{Sa1}$-Y88ONBY were each assayed in technical triplicate on two different days. Results are the average of the average rate for each batch of protein.

Calibration Plot. Fluorescence values for 1:1 molar mixtures of the cleavage products at 30 min after addition of $YoeB_{Sa1}$ were used to construct a calibration plot of picomoles of cleaved substrate versus relative fluorescence units (RFU). A separate calibration plot was constructed each time the fluorometric assay was performed.

Kinetic Analysis. In some of the progress curves, an increase in fluorescence was not observed until ∼15 min after the addition of $YoeB_{Sa1}$. However, the increase in measured fluorescence was linear over the majority of the remainder of the assay. Consequently, initial rates were calculated from the linear portion of the progress curves between 20 and 30 min. Fluorescence values were corrected by subtracting the fluorescence measured at 20 min from all subsequent time points. Corrected fluorescence values were converted to picomoles of cleaved substrate using the slope from the calibration plot, and linear regression was performed using Microsoft Excel to obtain initial velocities. Linear velocities were plotted versus substrate concentration, and the resulting data points were fit with the Hill equation using OriginPro version 8.0.

RESULTS

Prevalence, Conservation, and Transcription of *yefM-yoeB*$_{Sa1}$ and *yefM-yoeB*$_{Sa2}$ in MRSA Clinical Isolates. The artificial activation of TA systems is of significant interest as an intriguing antibacterial strategy.[11−14] $YoeB_{Sa1}$ and $YoeB_{Sa2}$ specifically present outstanding targets for this approach, as expression of $YoeB_{Sa1}$ and $YoeB_{Sa2}$ in the absence of their respective antitoxins, $YefM_{Sa1}$ and $YefM_{Sa2}$, induces growth arrest in *E. coli*.[28] For artificial activation of $YoeB_{Sa1}$ or $YoeB_{Sa2}$ to be an effective antibacterial strategy, YefM-$YoeB_{Sa1}$ and YefM-$YoeB_{Sa2}$ must be present and functional in clinical isolates of *S. aureus*. Thus, the presence, conservation, and transcription of *yefM-yoeB*$_{Sa1}$ and *yefM-yoeB*$_{Sa2}$ were investigated in a collection of 78 clinical isolates of MRSA from three Illinois hospitals and the Network on Antimicrobial Resistance in *S. aureus* (NARSA). Multiple-locus variable number of tandem repeats analysis previously confirmed that these isolates were not clonal.[21]

The total DNA of these isolates was probed for the presence of *yefM-yoeB*$_{Sa1}$ and *yefM-yoeB*$_{Sa2}$ using PCR with intragenic specific primers (Figure 1A). The *yefM-yoeB*$_{Sa1}$ and *yefM-yoeB*$_{Sa2}$ genes were present in 99% (77 of 78) of the clinical isolates (Table S2 of the Supporting Information). Approximately 10% of the PCR products were subjected to DNA sequencing, and the sequences were aligned with the reference genome from the *S. aureus* COL strain using CLUSTAL W[23] (Figures S1 and S2 of the Supporting Information) and compared with *yefM-yoeB*$_{Sa1}$ and *yefM-yoeB*$_{Sa2}$ loci from published *S. aureus* genomes using BLAST.[24] The *yefM-yoeB*$_{Sa1}$ PCR products were >97% identical with the *yefM-yoeB*$_{Sa1}$ genes in 29 of the 30 genomes containing that locus, while the *yefM-yoeB*$_{Sa2}$ PCR products were at least 96% identical with the *yefM-yoeB*$_{Sa2}$ genes in all 26 genomes containing that locus.

PCR products of ∼1.3 and ∼2.5 kb resulted from attempts to detect *yefM-yoeB*$_{Sa1}$ and *yefM-yoeB*$_{Sa2}$, respectively, in NRS27. DNA sequence analysis revealed that the product amplified by *yefM-yoeB*$_{Sa1}$-specific primers spanned a phage transcriptional repressor and a DNA polymerase III α subunit, while the product amplified by *yefM-yoeB*$_{Sa2}$-specific primers spanned an ornithine cyclodeaminase, a siderophore biosynthesis protein, and a multidrug resistance efflux pump. Sites of partial

dx.doi.org/10.1021/bi4008098 | *Biochemistry* 2014, 53, 188−201

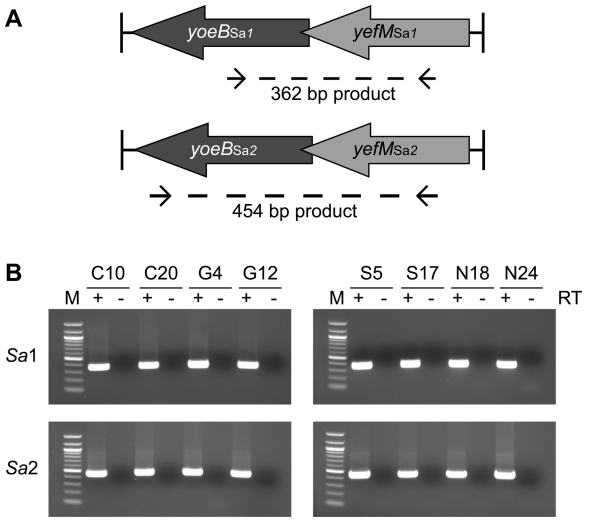

Figure 1. *yefM-yoeB*$_{Sa1}$ and *yefM-yoeB*$_{Sa2}$ are prevalent and transcribed in MRSA clinical isolates. (A) Locations of homology for primers used in PCR and RT-PCR. Primer sequences were designed from the *S. aureus* COL genome. (B) RT-PCR analysis of *yefM-yoeB*$_{Sa1}$ (*Sa*1, top two panels) and *yefM-yoeB*$_{Sa2}$ (*Sa*2, bottom two panels) transcription in MRSA clinical isolates. Lane M contains a DNA ladder [1517, 1200, 1000, 900, 800, 700, 600, 500, 400, 300, 200, and 100 bp (NEB)]. Plus and minus signs denote the inclusion and exclusion, respectively, of reverse transcriptase. Clinical isolates are identified by strain number.

complementarity were identified between the *yefM-yoeB*$_{Sa1}$- and *yefM-yoeB*$_{Sa2}$-specific primers and these genes, which could allow amplification in the absence of *yefM-yoeB*$_{Sa1}$ and *yefM-yoeB*$_{Sa2}$. To confirm the absence of *yefM-yoeB*$_{Sa1}$ and *yefM-yoeB*$_{Sa2}$ in NRS27, the *yefM*$_{Sa1}$, *yoeB*$_{Sa1}$, *yefM-yoeB*$_{Sa1}$, *yefM*$_{Sa2}$, *yoeB*$_{Sa2}$, and *yefM-yoeB*$_{Sa2}$ operons were individually amplified using primers designed to clone each of the full genes. PCR products were detected in the positive control strain NRS76, but not in NRS27. These results indicate that the *yefM-yoeB*$_{Sa1}$ and *yefM-yoeB*$_{Sa2}$ genes are not present in NRS27.

To investigate the transcription of *yefM-yoeB*$_{Sa1}$ and *yefM-yoeB*$_{Sa2}$ in MRSA, RT-PCR was performed on total RNA from eight isolates using the same primers used in the PCR screen. *yefM-yoeB*$_{Sa1}$ and *yefM-yoeB*$_{Sa2}$ were transcribed as bicistronic messages in each of the strains (Figure 1B). No PCR products were detected in the absence of reverse transcriptase, indicating the absence of DNA contamination. Taken together, these results suggest that *yefM-yoeB*$_{Sa1}$ and *yefM-yoeB*$_{Sa2}$ are widespread, conserved, and transcribed in clinical MRSA isolates. Thus, an activator of YoeB$_{Sa1}$ or YoeB$_{Sa2}$ with antibacterial activity could have broad efficacy against *S. aureus*.

Photocaging Allows Expression of YoeB$_{Sa1}$ in *E. coli*. YoeB$_{Ec}$ exhibits ribosome-dependent RNase activity *in vitro* and in *E. coli*.[20] YoeB$_{Sa1}$ and YoeB$_{Sa2}$ were found to exhibit RNase activity similar to that of YoeB$_{Ec}$ upon overexpression in *E. coli*, suggesting that they are ribosome-dependent RNases with the same mechanism of action as YoeB$_{Ec}$.[28] Intriguingly, YoeB$_{Ec}$ also possesses "residual" ribosome-independent RNase activity.[19] Evaluation of the possibility that YoeB$_{Sa1}$ and YoeB$_{Sa2}$ might also possess such activity necessitates the expression and purification of full-length, functional YoeB$_{Sa1}$ and YoeB$_{Sa2}$. However, YoeB$_{Sa1}$ and YoeB$_{Sa2}$ inhibit translation initiation and induce growth arrest in *E. coli*,[28] effectively preventing overexpression and characterization. As *yefM-yoeB*$_{Sa1}$ proved to be more amenable to manipulation using standard molecular biology techniques than *yefM-yoeB*$_{Sa2}$, a number of strategies were explored in efforts to obtain pure, functional YoeB$_{Sa1}$.

The most common method employed to obtain a functional TA system toxin for *in vitro* characterization involves co-expression of the antitoxin with the toxin, purification of the resulting TA complex, isolation of the toxin by denaturation of the complex, and subsequent refolding. Active YoeB$_{Ec}$ has been obtained by dissociation from YefM$_{Ec}$ in 6 M guanidine hydrochloride (GuHCl) followed by refolding via gradual dialysis into HEPES buffer.[19] YoeB$_{Ec}$ and YoeB$_{Sa1}$ share a high degree of sequence homology, suggesting that a similar method could allow purification of functional YoeB$_{Sa1}$. The *yefM-yoeB*$_{Sa1}$ operon was therefore cloned into pET-28a with a hexahistidine tag at the N-terminus of YefM$_{Sa1}$ to facilitate purification, and the complex was expressed in *E. coli* and purified using Ni-NTA resin. A variety of conditions were screened to identify an optimal method for denaturing, purifying, and refolding YoeB$_{Sa1}$. In each case, the YefM-YoeB$_{Sa1}$ complex was denatured by extended dialysis against either 6 M GuHCl or 8 M urea, YefM$_{Sa1}$ was extracted with Ni-NTA resin, and the presence and purity of the remaining YoeB$_{Sa1}$ were assessed using SDS−PAGE. If 6 M GuHCl was used as the denaturant, the recaptured YefM$_{Sa1}$ was highly pure, but YoeB$_{Sa1}$ was not recovered in the unbound fraction, probably because of the low initial ratio of YoeB$_{Sa1}$ to YefM$_{Sa1}$ and the necessity of diluting and precipitating samples containing GuHCl for SDS−PAGE. In contrast, when 8 M urea was used as the denaturant, YoeB$_{Sa1}$ was recovered, but a significant amount of residual YefM$_{Sa1}$ was also present. Efforts to refold the impure toxin by dilution or gradual dialysis resulted in substantial precipitation. These unpromising results led to the abandonment of denaturing purification and refolding as a viable approach to obtaining large quantities of pure, active YoeB$_{Sa1}$.

An alternative to denaturing purification of the toxin from the TA complex is to use a commercially available protease to selectively degrade the labile antitoxin from the TA complex, leaving the toxin unscathed.[27] The YefM-YoeB$_{Sa1}$ complex was expressed and purified as described above and subjected to digestion with trypsin. Analysis of the digest products by SDS−PAGE suggested that YoeB$_{Sa1}$ remained intact while YefM$_{Sa1}$ was rapidly and selectively degraded. However, the YoeB$_{Sa1}$ protein obtained from trypsin digestion of YefM-YoeB$_{Sa1}$ did not bind to YefM$_{Sa1}$ in pull-down experiments. Native PAGE of the digestion time course suggested that a fragment of YefM$_{Sa1}$ remained bound to YoeB$_{Sa1}$, prohibiting complex formation and indicating that this approach could not be used to obtain pure YoeB$_{Sa1}$.

The *yoeB*$_{Sa1}$ gene was then cloned at the C-terminus of glutathione *S*-transferase (GST) in hopes that a larger fusion partner would reduce the toxicity of YoeB$_{Sa1}$ by preventing it from binding to the ribosome. However, all sequenced clones contained frameshift mutations introducing premature stop codons in the *yoeB*$_{Sa1}$ gene. Two rounds of site-directed mutagenesis were performed to correct these mutations. Additional premature stop codons or inactivating mutations were introduced in each round, suggesting that low levels of full-length GST-YoeB$_{Sa1}$, produced by leaky expression from the T7 promoter even in the absence of T7 RNA polymerase, retained the ability to bind to the ribosome, inhibit translation, induce growth arrest, and prevent colony formation. Only mutant clones encoding premature stop codons were not toxic. These results hinted that the C-terminal region of YoeB$_{Sa1}$ is

dx.doi.org/10.1021/bi4008098 | *Biochemistry* 2014, 53, 188−201

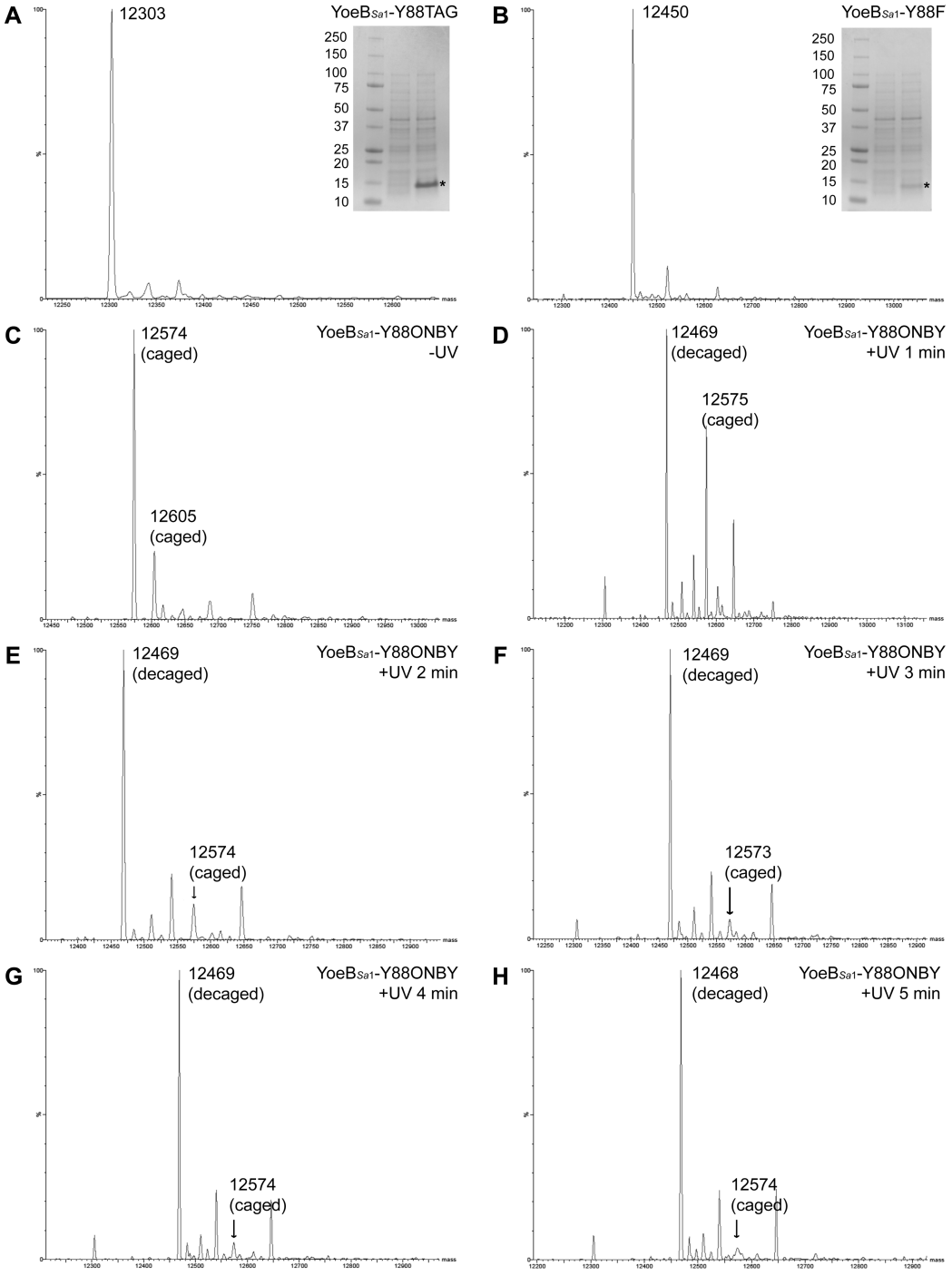

Figure 2. ESI-MS analysis of YoeB$_{Sa1}$ mutants. (A) YoeB$_{Sa1}$-Y88TAG (calculated molecular mass of 12307 Da and observed molecular mass of 12303 Da). (B) YoeB$_{Sa1}$-Y88F (calculated molecular mass of 12454 Da and observed molecular mass of 12450 Da). (A and B) Gel inset lanes: Kaleidoscope prestained standards (Bio-Rad), expression culture lysate immediately prior to induction with IPTG, and expression culture lysate 4 h postinduction (from left to right, respectively). The asterisk indicates the band corresponding to YoeB$_{Sa1}$-Y88TAG in panel A and YoeB$_{Sa1}$-Y88F in panel B. (C) YoeB$_{Sa1}$-Y88ONBY prior to exposure to UV light (calculated molecular mass of 12606 Da and observed molecular mass of 12574 Da). (D–H) YoeB$_{Sa1}$-Y88ONBY exposed to UV light for 1, 2, 3, 4, and 5 min, respectively (calculated molecular mass of 12470 Da and observed molecular mass of 12468–12469 Da).

necessary for activity and toxicity. As the C-terminal residues H83 and Y84 of YoeB$_{Ec}$ are required for both *in vitro* RNase activity and toxicity in *E. coli*,[19] the inability to clone the full-length *yoeB*$_{Sa1}$ gene at the C-terminus of GST suggested that the analogous H87 and Y88 in YoeB$_{Sa1}$ have similar roles.

Mutation of the C-terminal Y84 of YoeB$_{Ec}$ to phenylalanine or alanine was previously found to diminish both *in vitro* RNase activity and toxicity in *E. coli*,[19] suggesting that similar mutations to the homologous C-terminal Y88 of YoeB$_{Sa1}$ might sufficiently reduce toxicity to allow expression in *E. coli*. To investigate the contribution of Y88 to the toxicity of YoeB$_{Sa1}$, the TAT codon for Y88 in YoeB$_{Sa1}$ was changed to TAG for the amber stop codon (Y88TAG) or to TTT for phenylalanine (Y88F). The genes encoding these mutants were

dx.doi.org/10.1021/bi4008098 | *Biochemistry* 2014, 53, 188–201

cloned into pET-28a and expressed in *E. coli*. The resulting proteins were purified with yields of 5 mg of YoeB$_{Sa1}$-Y88TAG and 2.5 mg of YoeB$_{Sa1}$-Y88F per liter of culture. ESI mass spectrometry (ESI-MS) showed that the molecular masses of these mutants matched the predicted values [YoeB$_{Sa1}$-Y88TAG, expected molecular mass of 12307 Da and observed molecular mass of 12303 Da (Figure 2A); YoeB$_{Sa1}$-Y88F, expected molecular mass of 12454 Da and observed molecular mass of 12450 Da (Figure 2B)]. These results indicated that Y88 contributes to YoeB$_{Sa1}$ toxicity in *E. coli* and suggested that a nonpermanent modification of the structure of Y88 might sufficiently alleviate the toxicity of YoeB$_{Sa1}$ to allow expression of the full-length protein in *E. coli*.

Unnatural amino acid (UAA) mutagenesis allows the incorporation of a noncanonical amino acid site-specifically into a protein via the use of an aminoacyl-tRNA synthetase (aaRS)/tRNA pair that is orthogonal to the host organism's translational machinery.[29−31] The photocaged UAA *o*-nitrobenzyl tyrosine (ONBY) has been incorporated into a number of proteins in which a tyrosine is critical for enzymatic activity.[32−36] Mutation of tyrosine to ONBY "cages" the enzyme by inhibiting catalysis, substrate binding, or both. Irradiation with UV light between 300 and 365 nm releases the photocaging *o*-nitrobenzyl group,[37] revealing the free tyrosine and activating the enzyme for catalysis. As Y88 contributes to the toxicity and, presumably, the activity of YoeB$_{Sa1}$, it was hypothesized that mutation of Y88 to ONBY would allow expression of an inactive, nontoxic YoeB$_{Sa1}$ variant that could be activated by UV light following expression and purification.

The pEVOL plasmids for UAA mutagenesis encode an optimized amber (TAG) stop codon suppressor tRNA and two copies of an evolved UAA-specific *Methanocaldococcus jannaschii* aaRS, one under the control of a constitutive *glnS′* promoter and the other under the control of an arabinose-inducible *araBAD* promoter, which allows the expression level of the aaRS to be finely tuned.[38] As Y88 is the last residue in YoeB$_{Sa1}$, it would be challenging to purify ONBY-containing YoeB$_{Sa1}$ from prematurely truncated YoeB$_{Sa1}$. A variety of expression conditions were therefore screened by ESI-MS for maximal incorporation of ONBY into YoeB$_{Sa1}$. Maximal incorporation was achieved when 1 mM ONBY was present in the culture medium from the beginning of the expression, when aaRS expression was induced in early logarithmic growth phase, and when YoeB$_{Sa1}$ expression was induced in late logarithmic or early stationary phase and allowed to proceed overnight at 37 °C. Using this method, 1 mg of pure YoeB$_{Sa1}$-Y88ONBY was obtained per liter of culture. ESI-MS revealed that the mass of the full-length caged protein was ∼30 Da lower than predicted [YoeB$_{Sa1}$-Y88ONBY, expected molecular mass of 12606 Da and observed molecular mass of 12574 Da (Figure 2C)]. This discrepancy is attributed to reduction of the nitro group of ONBY to an amino group, a phenomenon that has been observed when ESI-MS is performed in protic solvents, resulting in a loss of 30 Da that corresponds to the observed mass shift.[39] Importantly, very little truncated YoeB$_{Sa1}$-Y88TAG was present (expected molecular mass of 12307 Da and observed molecular mass of 12305 Da). UV light-induced loss of the *o*-nitrobenzyl moiety was followed by ESI-MS [YoeB$_{Sa1}$-Y88, expected molecular mass of 12470 (Figure 2D−H)]. The extent of decaging increased as the extent of UV exposure was increased up to 3 min, after which no further decaging was observed (Figure 2F−H).

Decaged YoeB$_{Sa1}$ Is a Ribosome-Independent RNase. The ribosome-independent RNase activity of YoeB$_{Sa1}$ was assessed with respect to *yefM-yoeB*$_{Sa1}$ RNA *in vitro*. Decaging of YoeB$_{Sa1}$-Y88ONBY resulted in UV light-dependent degradation of the RNA (Figure 3A). In agreement with ESI-MS data

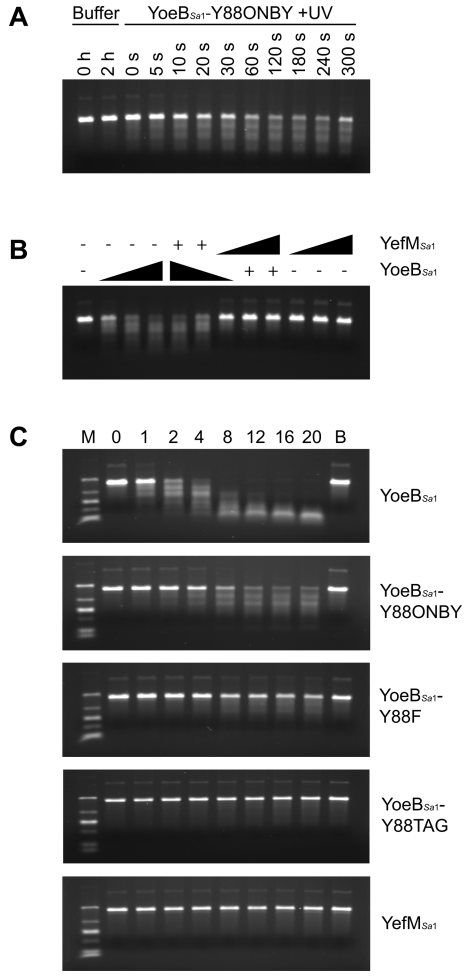

Figure 3. RNase activity of YoeB$_{Sa1}$ mutants. (A) RNase activity of YoeB$_{Sa1}$-Y88ONBY exposed to UV light for 0, 5, 10, 20, 30, 60, 120, 180, 240, or 300 s and incubated with *yefM-yoeB*$_{Sa1}$ RNA for 2 h. Buffer controls were incubated with *yefM-yoeB*$_{Sa1}$ RNA for 0 or 2 h. (B) Inhibition of YoeB$_{Sa1}$ by YefM$_{Sa1}$. YoeB$_{Sa1}$-Y88ONBY was exposed to UV light for 3 min. YefM$_{Sa1}$ and YoeB$_{Sa1}$ were mixed and incubated at 37 °C for 30 min to allow formation of the YefM-YoeB$_{Sa1}$ complex prior to incubation with *yefM-yoeB*$_{Sa1}$ RNA at 37 °C for 1 h. A minus sign designates 0 pmol of protein, a plus sign designates 10 pmol of protein, and right triangles designate increasing amounts of protein from 10 to 30 pmol. (C) RNase activity of YoeB$_{Sa1}$, YoeB$_{Sa1}$-Y88ONBY, YoeB$_{Sa1}$-Y88F, YoeB$_{Sa1}$-Y88TAG, and YefM$_{Sa1}$. Ten picomoles of protein was incubated with *yefM-yoeB*$_{Sa1}$ RNA for 0, 1, 2, 4, 8, 12, 16, or 20 h. Lane M contains an ssRNA ladder [1000, 500, 300, 150, 80, and 50 nucleotides (NEB)]. Lane B contains buffer and RNA at 20 h. In the top panel only, YoeB$_{Sa1}$-Y88ONBY was exposed to UV light for 3 min.

showing that the extent of decaging did not increase with additional UV exposure after 3 min (Figure 2F), the RNase activity of YoeB$_{Sa1}$-Y88ONBY also did not increase with additional UV exposure after 3 min (Figure 3A). YoeB$_{Sa1}$ activity was inhibited by the addition of an equimolar amount of YefM$_{Sa1}$ (Figure 3B), demonstrating that the observed RNase activity was due specifically to YoeB$_{Sa1}$ and not to RNase

dx.doi.org/10.1021/bi4008098 | *Biochemistry* 2014, 53, 188−201

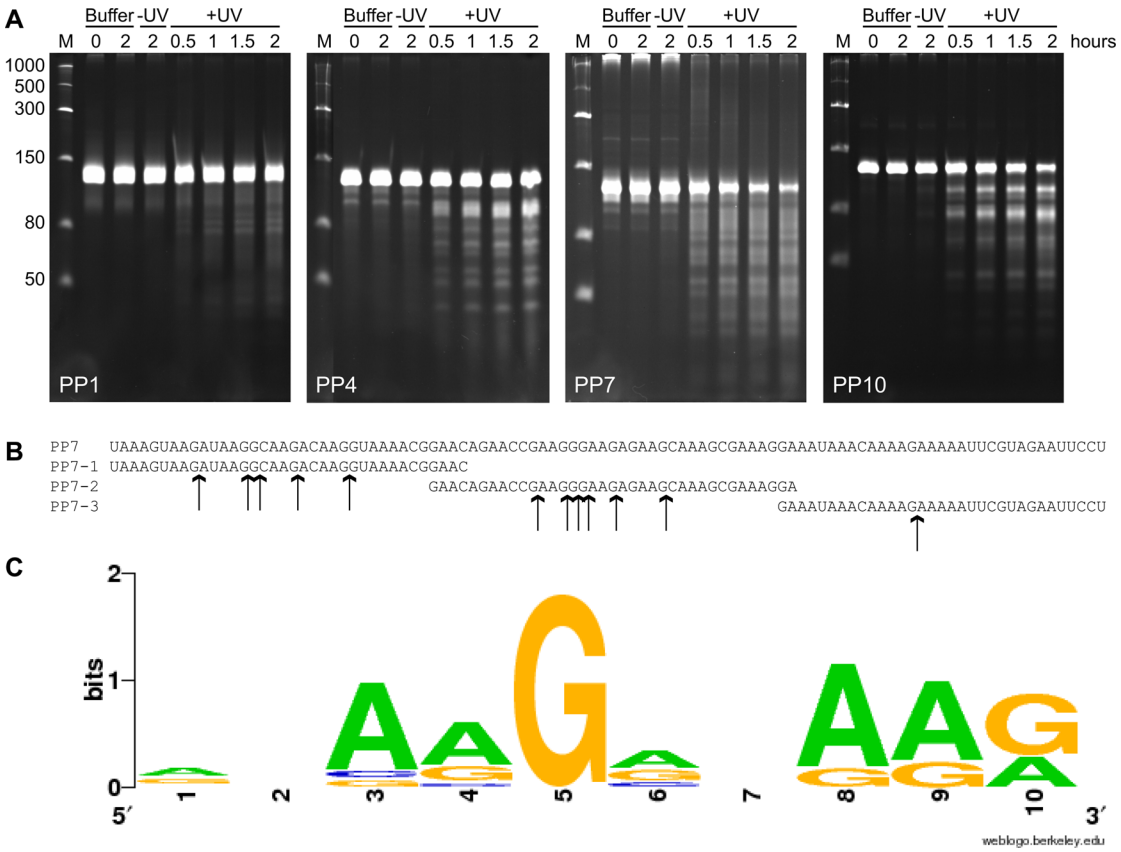

Figure 4. YoeB$_{Sa1}$ cleaves RNA at guanosine residues. (A) RNase activity of YoeB$_{Sa1}$ toward Pentaprobes 1, 4, 7, and 10. Lane M contains an ssRNA ladder [1000, 500, 300, 150, 80, and 50 nucleotides (NEB)]. In the buffer lanes, RNA was incubated in buffer alone for 0 or 2 h. In the −UV lanes, YoeB$_{Sa1}$-Y88ONBY was incubated with RNA for 2 h. In the +UV lanes, YoeB$_{Sa1}$-Y88ONBY was exposed to UV light for 2 min and incubated with RNA for 0.5, 1, 1.5, or 2 h. (B) Primary sequences of Pentaprobe 7 and Pentaprobe 7 oligonucleotides PP7-1, PP7-2, and PP7-3. YoeB$_{Sa1}$ cleavage sites identified by MALDI-MS are denoted with arrows. (C) YoeB$_{Sa1}$ consensus cleavage sequence calculated by WebLogo.[74]

contamination. This result also suggests that YefM$_{Sa1}$ inhibits YoeB$_{Sa1}$ at a 1:1 ratio, which is identical to the ratio of YefM$_{Ec}$ to YoeB$_{Ec}$ required to inhibit YoeB$_{Ec}$ in a similar *in vitro* assay.[19] Comparison of the activity of decaged YoeB$_{Sa1}$ with that of YoeB$_{Sa1}$ mutants and YefM$_{Sa1}$ reveals that YoeB$_{Sa1}$-Y88ONBY retains weak *in vitro* RNase activity, YoeB$_{Sa1}$-Y88F degrades RNA very slowly, and no detectable RNase activity is observed for YoeB$_{Sa1}$-Y88TAG or YefM$_{Sa1}$ (Figure 3C).

YoeB$_{Sa1}$ Cleaves RNA after Guanosine Residues. The Pentaprobes are a set of 12 plasmids that together encode every possible combination of five nucleotides in sequences of ∼100 nucleotides per plasmid.[40] The Pentaprobes have been used to determine the sequence specificity of RNases with recognition sequences of five or fewer nucleotides. Cleavage of each Pentaprobe by the RNase of interest is assessed by PAGE. Once cleaved Pentaprobes are identified, deconvolution occurs via MALDI-MS analysis of cleavage of small oligonucleotides.[27] The RNase activity of YoeB$_{Sa1}$ toward each of the 12 Pentaprobe RNA transcripts was assessed by denaturing PAGE. YoeB$_{Sa1}$ was least active toward Pentaprobe 1 and most active toward Pentaprobes 4, 7, and 10 (Figure 4A; other Pentaprobes not shown). Cleavage of Pentaprobe 7 was the most dramatic, with rapid and significant degradation of the full-length parent band and the appearance of a number of smaller discrete product bands, indicating that YoeB$_{Sa1}$ cleaves this Pentaprobe at multiple sites. The sequence of Pentaprobe 7 is rich in purine residues (Figure 4B), suggesting that the sequence specificity of YoeB$_{Sa1}$ might be similar to that of YoeB$_{Ec}$, which cleaves RNA after purine residues with a preference for adenosine.[19]

To identify the specific sequence recognized and cleaved by YoeB$_{Sa1}$ within Pentaprobe 7, cleavage of three overlapping oligonucleotides spanning Pentaprobe 7 (Figure 4B) was assessed by MALDI-MS. YoeB$_{Sa1}$ cleaved each oligonucleotide selectively after guanosine, leaving a 3′-cyclic phosphate on the 5′-RNA product. This suggests that YoeB$_{Sa1}$ is a guanosine-specific RNase *in vitro* and furthermore that the mechanism of YoeB$_{Sa1}$ RNA cleavage involves activation of the 2′-OH for nucleophilic attack of the 3′-phosphodiester bond. Fragments corresponding to both the 5′- and 3′-products were observed for 5 of the 9 guanosines in PP7-1, 6 of 13 in PP7-2, and 1 of 4 in PP7-3. Most of the noncleaved guanosines were near the termini of the oligonucleotides, which reduces the likelihood of observing cleavage at these sites by MALDI because of the 2 kDa lower mass limit of the detector and a reduction in MALDI sensitivity with an increase in oligonucleotide length. YoeB$_{Sa1}$ may also require a minimum number of residues 5′ or 3′ from the cleavage site to bind and cleave RNA and thus may skip guanosines near the termini of an oligonucleotide.

In the consensus sequence cleaved by YoeB$_{Sa1}$, adenosine residues precede and follow the guanosine at the cleavage site (Figure 4C). This may be an artifact of oligonucleotide design and selection, as most of the guanosines in Pentaprobe 7 are preceded by one or more adenosines. However, it is also possible that YoeB$_{Sa1}$ prefers to cleave after guanosines in the midst of purine-rich sequences. The fact that YoeB$_{Sa1}$ cleaved

dx.doi.org/10.1021/bi4008098 | *Biochemistry* 2014, 53, 188−201

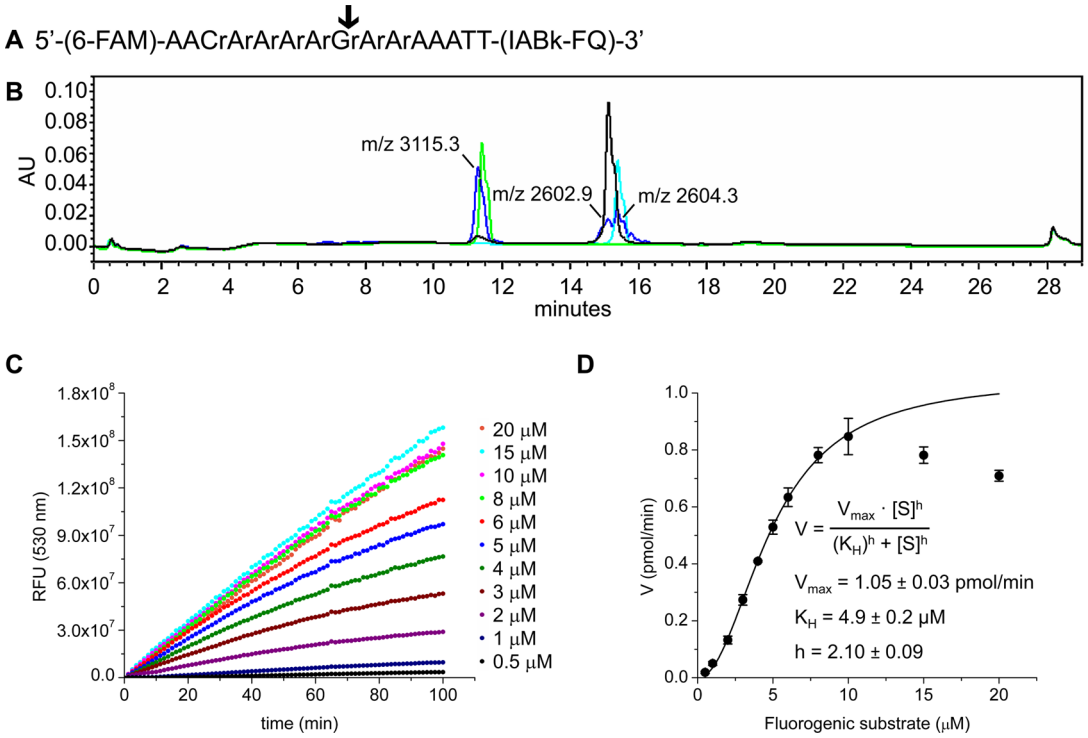

Figure 5. Kinetic analysis of YoeB$_{Sa1}$ using the fluorometric assay. (A) Fluorogenic substrate design. "r" designates RNA nucleotides. (B) HPLC traces of products of YoeB$_{Sa1}$ activity: black for 30 μM intact substrate, green for 30 μM 5′-cleavage product, cyan for 30 μM 3′-cleavage product, and blue for 30 μM substrate cleaved by 20 μM YoeB$_{Sa1}$ after 5 h at 25 °C. Peak fractions from the blue trace were analyzed by MALDI-MS and are labeled with the observed molecular masses of the 5′- and 3′-cleavage products (calculated molecular masses of 3115.0 Da and 2602.8 Da, respectively). (C) Representative set of progress curves from one experiment. (D) Initial slopes of fluorometric assay curves (●) with a Hill fit (—). Error bars represent the standard deviation (n = 3 separately purified batches of YoeB$_{Sa1}$, each assayed in technical triplicate on two different days; plotted data are the average of the average for each batch).

PP7-3 at only one of the three internal guanosines suggests that the ability of YoeB$_{Sa1}$ to cleave free mRNA may be inhibited by secondary structure, as PP7-3 had more predicted secondary structure than PP7-1 and PP7-2, which may have limited the ability of YoeB$_{Sa1}$ to access other potential cleavage sites in PP7-3.

Kinetic Characterization of YoeB$_{Sa1}$ RNase Activity. With the objective of developing a YoeB$_{Sa1}$ substrate that could be used to assess the activation of this RNase in a high-throughput setting, a fluorogenic oligonucleotide substrate was designed based on the data presented in Figure 4. An analogous design was previously used for the creation of a substrate for the ribosome-independent RNase MazF.[41,42] One of the sequences from PP7 that was cleaved by YoeB$_{Sa1}$ was converted into a 15-mer chimeric oligonucleotide with eight internal RNA residues surrounded by DNA nucleotides for stability (Figure 5A). Cleavage of this substrate was predicted to occur after the central guanosine residue. A 6-carboxyfluorescein fluorophore (excitation at 495 nm and emission at 520 nm) and an Iowa Black FQ quencher (absorbance maximum at 530 nm) were appended to the 5′- and 3′-ends, respectively, of the oligonucleotide. In the intact substrate, proximity allows the quencher to absorb the fluorescence emitted by the fluorophore. Cleavage of the substrate increases the distance between the fluorophore and the quencher, producing an increase in fluorescence that can be monitored spectrophotometrically.

The ability of YoeB$_{Sa1}$ to cleave this substrate was assessed by HPLC. The retention times of the products from YoeB$_{Sa1}$ activity overlapped with those of the independently synthesized standards (Figure 5B), suggesting that cleavage occurred primarily at guanosine, as predicted. MALDI-MS analysis of fractions collected from the elution peaks confirmed that the majority of cleavage events occurred at guanosine (Figure S3 of the Supporting Information). These results corroborate the guanosine specificity of YoeB$_{Sa1}$ ribosome-independent RNase activity.[19]

To determine the kinetic parameters of YoeB$_{Sa1}$ as a baseline for future high-throughput screening efforts, the RNase activity of YoeB$_{Sa1}$ toward the fluorogenic substrate was assessed in 384-well plate format. YoeB$_{Sa1}$ (5 μM) was incubated with a range of concentrations of the fluorogenic substrate (0.5−20 μM) to produce a set of progress curves (representative data from one replicate of one experiment shown in Figure 5C). For each experiment, a calibration curve was constructed by mixing the two chimeric products resulting from YoeB$_{Sa1}$ cleavage at a 1:1 molar ratio in the presence of YoeB$_{Sa1}$ (5 μM). The relationship between the measured fluorescence and the concentration of the cleavage products was linear up to 1.5 μM. This calibration curve was used to convert relative fluorescence units (RFU) at 530 nm to picomoles of cleaved substrate. Ideally, initial rates would be measured immediately following addition of YoeB$_{Sa1}$ to the substrate. However, in some experiments, a significant increase in fluorescence was not observed until ∼15 min after the addition of YoeB$_{Sa1}$. Consequently, the rates plotted in Figure 5D were determined from the linear portion of the progress curves between 20 and 30 min.

dx.doi.org/10.1021/bi4008098 | *Biochemistry* 2014, 53, 188−201

Traditional Michaelis–Menten enzyme kinetics are characterized by a hyperbolic rate, V, versus substrate concentration, [S], curve that can be fit by the equation

$$V = \frac{V_{max}[S]}{K_m + [S]} \quad (1)$$

where V_{max} is the maximal reaction velocity and K_m is the Michaelis constant, equal to the substrate concentration at which half-maximal activity is observed. This equation describes a hyperbolic rate that increases linearly when [S] is low and asymptotically approaches V_{max} at high values of [S].[43,44] The rate data in Figure 5D reveal that the kinetics of YoeB$_{Sa1}$ RNase activity toward the fluorogenic substrate are complex, with a sigmoidal increase in rate up to 10 μM substrate, followed by a marked decrease in rate at 15 and 20 μM substrate. The shape of the rate data suggests that the activity of YoeB$_{Sa1}$ is influenced by positive cooperativity at low substrate concentrations and by substrate inhibition at high substrate concentrations. However, careful consideration of the assay conditions and the nature of the fluorogenic substrate points to alternative explanations for the apparent cooperativity and substrate inhibition.

In traditional Michaelis–Menten enzyme kinetics, the substrate must be present in significant excess relative to the enzyme so that the substrate concentration is not substantially reduced by formation of the enzyme–substrate complex.[45] In the fluorometric assay, however, YoeB$_{Sa1}$ (5 μM) is present at a concentration similar to that of the fluorogenic substrate (0.5–20 μM) in each reaction. Rather than Michaelis–Menten conditions, these enzyme and substrate concentrations resemble those of mutual depletion systems, in which formation of the enzyme–substrate complex significantly reduces the concentrations of both the enzyme and the substrate.[46] Consequently, the classical Michaelis–Menten equation (eq 1) cannot be used to fit the kinetic data of YoeB$_{Sa1}$, but this does not necessarily mean that YoeB$_{Sa1}$ does not follow Michaelis–Menten kinetics. Interestingly, it has been shown that when the concentration of enzyme, $[E]_T$, is equal to or greater than the K_m, enzymes that follow Michaelis–Menten kinetics appear to have cooperative activity. The magnitude of the apparent cooperativity increases as $[E]_T$ increases relative to K_m, causing a concomitant increase in the substrate concentration $([S]_T)_{0.5}$ at which half-maximal velocity is observed.[47] This increase is given by eq 2:

$$([S]_T)_{0.5} = \frac{[E]_T}{2} + K_m \quad (2)$$

Eq 2 can be used to calculate K_m from a plot of reaction velocity versus substrate concentration for enzymes operating under mutual depletion conditions.[46,47]

However, the ability to calculate K_m using eq 2 depends on knowledge of V_{max}, which is required to estimate $([S]_T)_{0.5}$. The reduction in rate observed at 15 and 20 μM substrate precludes extrapolation to V_{max} from the kinetic plot and suggests the influence of substrate inhibition. However, this behavior is likely an artifact of the substrate design, in which a central guanosine RNA residue is flanked on both sides by three or four adenosine RNA residues (Figure 5A). These RNA residues could not be removed without abolishing the activity of YoeB$_{Sa1}$ toward the substrate. Although YoeB$_{Sa1}$ cleaves primarily after guanosine, minor cleavage is also observed after the neighboring adenosines (Figure S3 of the Supporting Information). As a result, the activity measured in the fluorometric assay is the sum of the rates at which YoeB$_{Sa1}$ cleaves after all of the RNA residues in the substrate. The preference for guanosine over adenosine suggests that cleavage after guanosine is faster than cleavage after adenosine. Thus, at nonsaturating substrate concentrations, the observed rate will be influenced primarily by cleavage after guanosine. As the substrate concentration increases, the proportion of cleavage events that are catalyzed after adenosine rather than guanosine will also increase. Eventually, at supersaturating substrate concentrations, the proportion of cleavage events at adenosine will increase to the degree that it will cause a measurable decrease in the overall rate, as observed in Figure 5D.

Consequently, V_{max} for guanosine-specific substrate cleavage cannot be determined from the kinetic data. However, assuming that cleavage after adenosine makes a limited contribution to the measured rate at low substrate concentrations, fitting the kinetic data at substrate concentrations below those at which a measurable decrease in rate occurs will allow extrapolation to an estimate for V_{max}. As it is possible that cleavage after adenosine makes a non-negligible contribution to the overall rate even at low substrate concentrations, this approach will provide minimal estimates only for V_{max} and K_m.

The Hill equation (eq 3) was originally derived to describe the cooperative binding of ligands to a protein containing multiple binding sites when one or more ligands are already bound:

$$\theta = \frac{[L]^h}{(K_A)^h + [L]^h} \quad (3)$$

where θ is the ratio of occupied binding sites to total binding sites, [L] is the ligand concentration, K_A is the association constant, and h is the Hill coefficient, which quantifies the degree of cooperativity.[48] The maximum possible value of h for a perfectly cooperative protein is equal to the number of ligand-binding sites. An h >1 indicates positive cooperativity, where the rate of ligand binding is enhanced by already bound ligands. An h <1 indicates negative cooperativity, where the rate of ligand binding is reduced by already bound ligands. An h equal to 1 indicates no cooperativity, where the rate of ligand binding is unaffected by already bound ligands. If h = 1, the Hill equation (eq 3) reduces to a form similar to that of the Michaelis–Menten equation (eq 1).[44]

In addition to ligand-binding proteins, many enzymes exhibit cooperative enhancements or reductions in rate that result from conformational changes induced by enzyme oligomerization or the binding of allosteric effectors. Another smaller but growing class of monomeric enzymes with single ligand-binding sites also exhibits cooperative behavior caused by conformational transformations between two or more enzyme forms with differing substrate affinities. If the rate of conformational interconversion is slower than the rate of the reaction, substrate binding cannot reach equilibrium, resulting in nonhyperbolic, non-Michaelis–Menten kinetics.[49]

Therefore, an alternative to mutual depletion as an explanation for the sigmoidal kinetics of YoeB$_{Sa1}$ is that its activity is cooperative, which would require oligomerization, allosteric effector binding, or a slow conformational change. Comparison of the gel filtration elution volume of YoeB$_{Sa1}$ with those of known standards indicates that YoeB$_{Sa1}$ is monomeric under the conditions employed in this assay. Furthermore, the assay buffer contains no known allosteric effectors, indicating

dx.doi.org/10.1021/bi4008098 | Biochemistry 2014, 53, 188–201

that oligomerization and effector binding are unlikely to be responsible for the sigmoidal shape of the kinetic data. On the other hand, the crystal structures of YefM-YoeB$_{Ec}$ and YoeB$_{Ec}$ reveal that YefM$_{Ec}$ induces a conformational change in the active site of YoeB$_{Ec}$,[19] which suggests that this area may be conformationally flexible. Moreover, as the primary cellular function of YoeB homologues appears to be ribosome-dependent RNase activity,[20,28,50−52] the conformation of YoeB$_{Sa1}$ that cleaves RNA in a ribosome-dependent fashion may be distinct from the conformations that exist free in solution and cleave free mRNA. Slow conformational change is therefore a plausible explanation for the observed cooperativity in the kinetics of YoeB$_{Sa1}$ activity toward the fluorogenic substrate.

Regardless of whether the sigmoidal shape of the kinetic data results from mutual depletion or monomeric cooperativity, a modified version of the Hill equation can be used to provide a minimal estimate for V_{max}. The simplest and most common method applied in the analysis of the kinetics of cooperative monomeric enzymes with single ligand-binding sites is a combination of the Hill and Michaelis−Menten equations:

$$V = \frac{V_{max}[S]^h}{(K_H)^h + [S]^h} \quad (4)$$

where V_{max} is the maximal reaction velocity, [S] is the substrate concentration, K_H is the substrate concentration at which half-maximal activity is observed, and h is the Hill coefficient.[49] If YoeB$_{Sa1}$ is cooperative, h quantifies the degree of cooperativity, and K_H is equivalent to K_m. On the other hand, if mutual depletion occurs, h quantifies the deviation from hyperbolic Michaelis−Menten kinetics, and K_m can be calculated using eq 2 with $K_H = ([S]_T)_{0.5}$. Eq 4 was therefore used to fit the kinetic data for substrate concentrations between 0.5 and 10 μM to allow extrapolation to a minimal estimate for V_{max}. This gave a V_{max} of 1.05 ± 0.03 pmol/min and a K_H of 4.9 ± 0.2 μM, with an h of 2.10 ± 0.09 (Figure 5D). Using $K_H = ([S]_T)_{0.5}$ in eq 2 gives a K_m of 2.4 ± 0.2 μM.

DISCUSSION

The YoeB$_{Sa1}$ and YoeB$_{Sa2}$ toxins from *S. aureus* were previously found to induce growth arrest and to exhibit cellular RNase activity identical to that of YoeB$_{Ec}$ upon overexpression in *E. coli*.[28] As YoeB$_{Ec}$ possesses weak ribosome-independent RNase activity with a preference for purine nucleotides *in vitro*,[19] the possibility that YoeB$_{Sa1}$ also has ribosome-independent RNase activity was investigated.

One of the most significant obstacles to characterizing the activities and determining the structures of toxic proteins is the difficulty of overexpression in heterologous hosts such as *E. coli*. Many TA system toxins cannot be obtained in sufficient quantities for characterization because their overexpression arrests growth and/or kills the cells. After the failure of multiple strategies to provide pure, full-length, functional YoeB$_{Sa1}$, the discovery that Y88 is required for YoeB$_{Sa1}$ toxicity in *E. coli* led to the utilization of UAA mutagenesis to replace this residue with the photocaged amino acid ONBY, which reduced the toxicity of YoeB$_{Sa1}$ to a sufficient degree to allow overexpression in *E. coli*.

To the best of our knowledge, this is the first reported use of *in vivo* UAA mutagenesis to facilitate the isolation and characterization of a toxin from a TA system. Incorporation of ONBY has also been used to overexpress a toxic zinc-finger nuclease in an inactive, nontoxic form in *E. coli*,[36] suggesting that incorporation of a photocaged version of a critical catalytic residue via UAA mutagenesis may provide a general strategy for allowing expression and characterization of toxic enzymes, provided that an appropriate aaRS/tRNA pair is available. For example, Y87 in YoeB$_{Sa2}$ is homologous to Y88 in YoeB$_{Sa1}$ and appears to be important for YoeB$_{Sa2}$ toxicity in *E. coli* (unpublished data). Consequently, incorporation of ONBY into YoeB$_{Sa2}$ using UAA mutagenesis may allow expression of YoeB$_{Sa2}$ in *E. coli* for *in vitro* characterization as well. Furthermore, aaRS/tRNA pairs have also been developed for photocaged cysteine, serine, and lysine.[31] Photocaged versions of aspartate, glutamate, glycine, alanine, and histidine have been synthesized,[53−55] but corresponding aaRS/tRNA pairs do not yet exist. A list of residues identified by mutagenesis and structural data to be responsible for the activity and/or toxicity of a number of TA system toxins is provided in Table 1.

Table 1. Residues Responsible for the Activity and/or Toxicity of Various TA System Toxins

toxin	source(s)	residues implicated in activity and/or toxicity
CcdB[57,58]	*Aliivibrio fischeri*, plasmid F	Trp99, Gly100, Ile101
Doc[59]	Plasmid P1	His66, Asp70
FitB[60]	*Neisseria gonorrheae*	Asp5, Glu42, Asp104, Asp122
HigB[61]	*Proteus* spp.	His92
HipA[62]	*E. coli*	Ser150, Asp209, Asp332
Kid[63]	*E. coli*	Asp75, Arg73, His17
MazF[64]	*E. coli*	Glu24, His28
MqsR[65]	*E. coli*	Lys56, Gln68, Tyr81, Lys96
PemK[66]	*Bacillus anthracis*	Glu24, His59
PezT[67,68]	*Streptococcus pneumoniae*	Lys45, Asp66, Thr118, Arg157, Arg170
RelE[56]	*E. coli*	Arg61, Arg81, Tyr87
VapC-3[69]	*Mycobacterium tuberculosis*	Asp9, Glu43, Asp99, Asp117
VapC-5[70]	*M. tuberculosis*	Asp26, Glu57, Asp115, Asp135
VapC[71]	*Shigella flexneri*	Asp7, Glu42, Asp98
YafQ[72]	*E. coli*	His50, His63, Asp67, Trp68, Arg83, His87, Phe91
YoeB[19]	*E. coli*	Glu46, Arg65, His83, Tyr88
ζ[73]	*Streptococcus pyogenes*	Lys46, Asp67

Notably, each characterized toxin possesses one or more residues corresponding to an accessible photocaged amino acid. Introduction of aaRS/tRNA pairs specific for photocaged aspartate and histidine could allow for the general application of the photocaging strategy for expressing these proteins and studying their activities and cellular roles *in vitro* and in cells.

YoeB$_{Ec}$ belongs to the RelE structural family. RelE is a ribosome-dependent RNase toxin that is active only in the presence of the ribosome. In the ribosome-bound structure of RelE, Y87 of RelE stacks with the residue upstream of the cleavage site, and its hydroxyl is the closest functional group to the 2′-OH of the cleaved residue, suggesting a dual role in substrate binding and catalysis. Y87 is hypothesized to act as a general base through hydrogen bonding to a water molecule, causing the deprotonation and activation of the 2′-OH for attack of the 3′-phosphodiester bond.[56] The role of Y88 in the catalytic mechanism of YoeB$_{Sa1}$ is currently unknown and may be different in the presence and absence of the ribosome. Mutation of Y88 in YoeB$_{Sa1}$-Y88TAG, YoeB$_{Sa1}$-Y88F, and YoeB$_{Sa1}$-Y88ONBY sufficiently reduced cellular toxicity to allow overexpression in *E. coli* (Figure 2). The relative yields

of YoeB$_{Sa1}$-Y88TAG (5 mg/L) and YoeB$_{Sa1}$-Y88F (2.5 mg/L) under identical expression conditions indicate that the Y88TAG mutation renders YoeB$_{Sa1}$ less toxic than the Y88F mutation, which suggests that both the aromatic ring and hydroxyl functional group of Y88 contribute to cellular RNase activity. Similarly, YoeB$_{Sa1}$-Y88F and YoeB$_{Sa1}$-Y88ONBY retained the capacity to cleave free mRNA *in vitro*, albeit at a significantly reduced rate and to a much lesser extent than decaged YoeB$_{Sa1}$, while the RNase activity of YoeB$_{Sa1}$-Y88TAG was almost completely abolished (Figure 3C). These results suggest that both the aromatic ring and hydroxyl functional group of Y88 also contribute to the *in vitro* activity of YoeB$_{Sa1}$, although the exact role played by each of these moieties in ribosome-independent RNase activity remains unknown.

YoeB$_{Ec}$ was previously found to possess purine-specific ribosome-independent RNase activity with a preference for adenosine over guanosine.[19] In contrast, YoeB$_{Sa1}$ preferentially cleaves free mRNA after guanosine and to a much lesser extent after adenosine (Figures 4B and 5B and Figure S3 of the Supporting Information). This specificity was used to design a chimeric fluorogenic substrate to study the kinetics of YoeB$_{Sa1}$ activity. The resulting kinetic data show a sigmoidal increase in rate at low substrate concentrations followed by a decrease at high substrate concentrations. There are several plausible explanations for these deviations from standard hyperbolic Michaelis−Menten kinetics. First, the sigmoidal shape of the kinetic data may be an artifact of the high enzyme concentration used in these experiments,[47] as it was necessary for the concentrations of YoeB$_{Sa1}$ and the fluorogenic substrate to be roughly equal (5 and 0.5−20 μM, respectively) to observe YoeB$_{Sa1}$ activity using the fluorometric assay. Alternatively, a slow transition between inactive and active enzyme conformations may be required for catalysis, resulting in a failure to achieve a steady state of the bound substrate due to the faster speed of enzymatic catalysis. The seeming substrate inhibition is likely an artifact resulting from the unavoidable inclusion of adenosine RNA residues bordering guanosine in the substrate. Cleavage at these adenosine residues is hypothesized to cause a measurable reduction in rate at high substrate concentrations, necessitating the exclusion of these points from the kinetic analysis. It should be noted that these explanations are not mutually exclusive, and two or all three could conceivably be involved in the complex kinetics of YoeB$_{Sa1}$ activity toward the fluorogenic substrate. The Hill equation was used to fit the sigmoidal portion of the kinetic data to provide minimal estimates for V_{max} and K_m. Fitting the kinetic data with the Hill equation (eq 4) for cooperative enzymatic activity gave a V_{max} of 1.05 ± 0.03 pmol/min, a K_H of 4.9 ± 0.2 μM, and a Hill coefficient h of 2.10 ± 0.09 (Figure 5D). Using eq 2 to convert K_H to K_m gives a K_m of 2.4 ± 0.2 μM.

The relatively low affinity and slow rate observed for YoeB$_{Sa1}$ cleavage of free mRNA suggest that ribosome-independent RNase activity is unlikely to make a significant contribution to the activity of YoeB$_{Sa1}$ in cells. This is consistent with prior evidence of only ribosome-dependent RNase activity upon overexpression of YoeB$_{Sa1}$ in *E. coli*.[28] YoeB$_{Ec}$ is structurally homologous to RNase Sa from *Streptomyces aureofaciens* and Barnase from *Bacillus amyloliquefaciens*, both of which are guanosine-specific RNases,[19] and the catalytic Glu-Arg-His triad found in these and other microbial guanosine-specific RNases is conserved in YoeB$_{Ec}$, YoeB$_{Sa1}$, and YoeB$_{Sa2}$. However, YoeB homologues lack a C-terminal extension that orients the nucleotide downstream of the cleavage site via stacking interactions with aromatic side chains. Ribosomal nucleotides may supply these interactions to facilitate proper orientation and cleavage of bound mRNA when YoeB binds in the ribosome, as in the crystal structure of the RelE−ribosome complex.[56] The absence of the C-terminal extension and ribosomal interactions may explain the low affinity and slow rate of the RNase activity of free YoeB$_{Sa1}$.

Although YoeB$_{Ec}$ was originally found to have ribosome-independent RNase activity in *in vitro* experiments,[19] the only cellular RNase activity observed for YoeB homologues has been ribosome-dependent.[20,28,50−52] This suggests that the ribosome-independent RNase activity of YoeB$_{Sa1}$ described here may have little relevance in cells apart from the discovery of an artificial activator capable of stabilizing a ribosome-independent RNase conformation of YoeB$_{Sa1}$. Then activation of YoeB$_{Sa1}$ from the YefM−YoeB$_{Sa1}$ complex in *S. aureus* could lead to global nonspecific RNA degradation via the guanosine-specific ribosome-independent RNase activity reported here, in addition to translation inhibition via the ribosome-dependent RNase activity described previously,[28] causing growth arrest and possibly eventual death. The fluorometric assay developed for YoeB$_{Sa1}$ ribosome-independent RNase activity will facilitate high-throughput screens of chemical and peptide libraries to identify molecules capable of activating YoeB$_{Sa1}$ via prevention of YefM-YoeB$_{Sa1}$ complex formation or disruption of the complex.

■ ASSOCIATED CONTENT

Supporting Information

Two tables listing the primers used in this study (Table S1) and the results of the PCR screen for *yefM-yoeB*$_{Sa1}$ and *yefM-yoeB*$_{Sa2}$ in MRSA clinical isolates (Table S2) as well as three figures showing the sequence alignments of *yefM-yoeB*$_{Sa1}$ (Figure S1) and *yefM-yoeB*$_{Sa2}$ (Figure S2) PCR products and the MALDI spectra of the fluorogenic substrate cleavage products (Figure S3). This material is available free of charge via the Internet at http://pubs.acs.org.

■ AUTHOR INFORMATION

Corresponding Author

*E-mail: hergenro@illinois.edu. Phone: (217) 333-0363.

Funding

This work was supported by National Institutes of Health (NIH) Grant 2R01-GM068385 to P.J.H. A.S.L. was partially supported by an NIH Chemistry-Biology Interface Training Grant (National Institute of General Medical Sciences Grant 5T32-GM070421).

Notes

The authors declare no competing financial interest.

■ ACKNOWLEDGMENTS

We thank Prof. Peter Schultz at the Scripps Research Institute (La Jolla, CA) for providing pEVOL-ONBY and Prof. Joel Mackay at the University of Sydney (Sydney, Australia) for providing the Pentaprobes. We also thank Prof. Alex Deiters and Jessica Torres Kolbus at North Carolina State University (Raleigh, NC) for advice regarding the synthesis of ONBY.

■ ABBREVIATIONS

TA, toxin−antitoxin; RNase, ribonuclease; ONBY, *o*-nitrobenzyl tyrosine.

REFERENCES

(1) Pandey, D. P., and Gerdes, K. (2005) Toxin-antitoxin loci are highly abundant in free-living but lost from host-associated prokaryotes. *Nucleic Acids Res. 33*, 966−976.

(2) Yamaguchi, Y., Park, J. H., and Inouye, M. (2011) Toxin-antitoxin systems in bacteria and archaea. *Annu. Rev. Genet. 45*, 61−79.

(3) Masuda, H., Tan, Q., Awano, N., Wu, K. P., and Inouye, M. (2012) YeeU enhances the bundling of cytoskeletal polymers of MreB and FtsZ, antagonizing the CbtA (YeeV) toxicity in *Escherichia coli*. *Mol. Microbiol. 84*, 979−989.

(4) Wang, X., Lord, D. M., Cheng, H. Y., Osbourne, D. O., Hong, S. H., Sanchez-Torres, V., Quiroga, C., Zheng, K., Herrmann, T., Peti, W., Benedik, M. J., Page, R., and Wood, T. K. (2012) A new type V toxin-antitoxin system where mRNA for toxin GhoT is cleaved by antitoxin GhoS. *Nat. Chem. Biol. 8*, 855−861.

(5) Gerdes, K., Christensen, S. K., and Lobner-Olesen, A. (2005) Prokaryotic toxin-antitoxin stress response loci. *Nat. Rev. Microbiol. 3*, 371−382.

(6) Gerdes, K., Rasmussen, P. B., and Molin, S. (1986) Unique type of plasmid maintenance function: Postsegregational killing of plasmid-free cells. *Proc. Natl. Acad. Sci. U.S.A. 83*, 3116−3120.

(7) Leplae, R., Geeraerts, D., Hallez, R., Guglielmini, J., Dreze, P., and Van Melderen, L. (2011) Diversity of bacterial type II toxin-antitoxin systems: A comprehensive search and functional analysis of novel families. *Nucleic Acids Res. 39*, 5513−5525.

(8) Magnuson, R. D. (2007) Hypothetical functions of toxin-antitoxin systems. *J. Bacteriol. 189*, 6089−6092.

(9) Schuster, C. F., and Bertram, R. (2013) Toxin-antitoxin systems are ubiquitous and versatile modulators of prokaryotic cell fate. *FEMS Microbiol. Lett. 340*, 73−85.

(10) Pedersen, K., Christensen, S. K., and Gerdes, K. (2002) Rapid induction and reversal of a bacteriostatic condition by controlled expression of toxins and antitoxins. *Mol. Microbiol. 45*, 501−510.

(11) Engelberg-Kulka, H., Sat, B., Reches, M., Amitai, S., and Hazan, R. (2004) Bacterial programmed cell death systems as targets for antibiotics. *Trends Microbiol. 12*, 66−71.

(12) DeNap, J. C., and Hergenrother, P. J. (2005) Bacterial death comes full circle: Targeting plasmid replication in drug-resistant bacteria. *Org. Biomol. Chem. 3*, 959−966.

(13) Williams, J. J., and Hergenrother, P. J. (2008) Exposing plasmids as the Achilles' heel of drug-resistant bacteria. *Curr. Opin. Chem. Biol. 12*, 389−399.

(14) Williams, J. J., and Hergenrother, P. J. (2012) Artificial activation of toxin-antitoxin systems as an antibacterial strategy. *Trends Microbiol. 20*, 291−298.

(15) Diekema, D. J., Pfaller, M. A., Schmitz, F. J., Smayevsky, J., Bell, J., Jones, R. N., and Beach, M. (2001) Survey of infections due to *Staphylococcus* species: Frequency of occurrence and antimicrobial susceptibility of isolates collected in the United States, Canada, Latin America, Europe, and the Western Pacific region for the SENTRY Antimicrobial Surveillance Program, 1997−1999. *Clin. Infect. Dis. 32* (Suppl. 2), S114−S132.

(16) Donegan, N. P., and Cheung, A. L. (2009) Regulation of the *mazEF* toxin-antitoxin module in *Staphylococcus aureus* and its impact on *sigB* expression. *J. Bacteriol. 191*, 2795−2805.

(17) Donegan, N. P., Thompson, E. T., Fu, Z., and Cheung, A. L. (2010) Proteolytic regulation of toxin-antitoxin systems by ClpPC in *Staphylococcus aureus*. *J. Bacteriol. 192*, 1416−1422.

(18) Makarova, K. S., Wolf, Y. I., and Koonin, E. V. (2009) Comprehensive comparative-genomic analysis of type 2 toxin-antitoxin systems and related mobile stress response systems in prokaryotes. *Biol. Direct 4*, 19.

(19) Kamada, K., and Hanaoka, F. (2005) Conformational change in the catalytic site of the ribonuclease YoeB toxin by YefM antitoxin. *Mol. Cell 19*, 497−509.

(20) Zhang, Y., and Inouye, M. (2009) The inhibitory mechanism of protein synthesis by YoeB, an *Escherichia coli* toxin. *J. Biol. Chem. 284*, 6627−6638.

(21) Williams, J. J., Halvorsen, E. M., Dwyer, E. M., DiFazio, R. M., and Hergenrother, P. J. (2011) Toxin-antitoxin (TA) systems are prevalent and transcribed in clinical isolates of *Pseudomonas aeruginosa* and methicillin-resistant *Staphylococcus aureus*. *FEMS Microbiol. Lett. 322*, 41−50.

(22) Moritz, E. M., and Hergenrother, P. J. (2007) Toxin-antitoxin systems are ubiquitous and plasmid-encoded in vancomycin-resistant enterococci. *Proc. Natl. Acad. Sci. U.S.A. 104*, 311−316.

(23) Thompson, J. D., Higgins, D. G., and Gibson, T. J. (1994) CLUSTAL W: Improving the sensitivity of progressive multiple sequence alignment through sequence weighting, position-specific gap penalties and weight matrix choice. *Nucleic Acids Res. 22*, 4673−4680.

(24) Altschul, S. F., Gish, W., Miller, W., Myers, E. W., and Lipman, D. J. (1990) Basic local alignment search tool. *J. Mol. Biol. 215*, 403−410.

(25) Miller, J. C., Silverman, S. K., England, P. M., Dougherty, D. A., and Lester, H. A. (1998) Flash decaging of tyrosine sidechains in an ion channel. *Neuron 20*, 619−624.

(26) Wessel, D., and Flugge, U. I. (1984) A method for the quantitative recovery of protein in dilute solution in the presence of detergents and lipids. *Anal. Biochem. 138*, 141−143.

(27) McKenzie, J. L., Duyvestyn, J. M., Smith, T., Bendak, K., Mackay, J., Cursons, R., Cook, G. M., and Arcus, V. L. (2012) Determination of ribonuclease sequence-specificity using Pentaprobes and mass spectrometry. *RNA 18*, 1267−1278.

(28) Yoshizumi, S., Zhang, Y., Yamaguchi, Y., Chen, L., Kreiswirth, B. N., and Inouye, M. (2009) *Staphylococcus aureus* YoeB homologues inhibit translation initiation. *J. Bacteriol. 191*, 5868−5872.

(29) Wang, L., Brock, A., Herberich, B., and Schultz, P. G. (2001) Expanding the genetic code of *Escherichia coli*. *Science 292*, 498−500.

(30) Liu, C. C., and Schultz, P. G. (2010) Adding new chemistries to the genetic code. *Annu. Rev. Biochem. 79*, 413−444.

(31) Davis, L., and Chin, J. W. (2012) Designer proteins: Applications of genetic code expansion in cell biology. *Nat. Rev. Mol. Cell Biol. 13*, 168−182.

(32) Deiters, A., Groff, D., Ryu, Y., Xie, J., and Schultz, P. G. (2006) A genetically encoded photocaged tyrosine. *Angew. Chem., Int. Ed. 45*, 2728−2731.

(33) Chou, C., Young, D. D., and Deiters, A. (2009) A light-activated DNA polymerase. *Angew. Chem., Int. Ed. 48*, 5950−5953.

(34) Edwards, W. F., Young, D. D., and Deiters, A. (2009) Light-activated Cre recombinase as a tool for the spatial and temporal control of gene function in mammalian cells. *ACS Chem. Biol. 4*, 441−445.

(35) Chou, C., Young, D. D., and Deiters, A. (2010) Photocaged T7 RNA polymerase for the light activation of transcription and gene function in pro- and eukaryotic cells. *ChemBioChem 11*, 972−977.

(36) Chou, C., and Deiters, A. (2011) Light-activated gene editing with a photocaged zinc-finger nuclease. *Angew. Chem., Int. Ed. 50*, 6839−6842.

(37) Zhao, H., Sterner, E. S., Coughlin, E. B., and Theato, P. (2012) o-Nitrobenzyl alcohol derivatives: Opportunities in polymer and materials science. *Macromolecules 45*, 1723−1736.

(38) Young, T. S., Ahmad, I., Yin, J. A., and Schultz, P. G. (2010) An enhanced system for unnatural amino acid mutagenesis in *E. coli*. *J. Mol. Biol. 395*, 361−374.

(39) Karancsi, T., and Slegel, P. (1999) Reliable molecular mass determination of aromatic nitro compounds: Elimination of gas-phase reduction occurring during atmospheric pressure chemical ionization. *J. Mass Spectrom. 34*, 975−977.

(40) Bendak, K., Loughlin, F. E., Cheung, V., O'Connell, M. R., Crossley, M., and Mackay, J. P. (2012) A rapid method for assessing the RNA-binding potential of a protein. *Nucleic Acids Res. 40*, e105.

(41) Wang, N. R., and Hergenrother, P. J. (2007) A continuous fluorometric assay for the assessment of MazF ribonuclease activity. *Anal. Biochem. 371*, 173−183.

(42) van Rensburg, J. J., and Hergenrother, P. J. (2013) Detection of endogenous MazF enzymatic activity in *Staphylococcus aureus*. *Anal. Biochem. 443*, 81−87.

(43) Michaelis, L., Menten, M. L., Johnson, K. A., and Goody, R. S. (2011) The original Michaelis constant: Translation of the 1913 Michaelis-Menten paper. *Biochemistry 50*, 8264−8269.
(44) Nelson, D. L., Lehninger, A. L., and Cox, M. M. (2008) *Lehninger Principles of Biochemistry*, 5th ed., W. H. Freeman, New York.
(45) Schnell, S., and Maini, P. K. (2003) A century of enzyme kinetics: Reliability of the K_m and V_{max} estimates. *Comments on Theoretical Biology 8*, 169−187.
(46) Griffiths, J. R. (1979) Steady-state enzyme kinetics in mutual depletion systems. *Biochem. Soc. Trans. 7*, 429−439.
(47) Laurent, M., and Kellershohn, N. (1984) Apparent co-operativity for highly concentrated Michaelian and allosteric enzymes. *J. Mol. Biol. 174*, 543−555.
(48) Hill, A. V. (1910) The possible effects of the aggregation of the molecules of haemoglobin on its dissociation curves. *J. Physiol. 40*, iv−vii.
(49) Porter, C. M., and Miller, B. G. (2012) Cooperativity in monomeric enzymes with single ligand-binding sites. *Bioorg. Chem. 43*, 44−50.
(50) Halvorsen, E. M., Williams, J. J., Bhimani, A. J., Billings, E. A., and Hergenrother, P. J. (2011) Txe, an endoribonuclease of the enterococcal Axe-Txe toxin-antitoxin system, cleaves mRNA and inhibits protein synthesis. *Microbiology 157*, 387−397.
(51) Sevillano, L., Diaz, M., Yamaguchi, Y., Inouye, M., and Santamaria, R. I. (2012) Identification of the first functional toxin-antitoxin system in *Streptomyces*. *PLoS One 7*, e32977.
(52) Nolle, N., Schuster, C. F., and Bertram, R. (2013) Two paralogous *yefM-yoeB* loci from *Staphylococcus equorum* encode functional toxin-antitoxin systems. *Microbiology 159* (Part 8), 1575−1585.
(53) Wilcox, M., Viola, R. W., Johnson, K. W., Billington, A. P., Carpenter, B. K., Mccray, J. A., Guzikowski, A. P., and Hess, G. P. (1990) Synthesis of photolabile precursors of amino-acid neurotransmitters. *J. Org. Chem. 55*, 1585−1589.
(54) Zhang, Z., Papageorgiou, G., Corrie, J. E. T., and Grewer, C. (2007) Pre-steady-state currents in neutral amino acid transporters induced by photolysis of a new caged alanine derivative. *Biochemistry 46*, 3872−3880.
(55) Nakayama, K., Heise, I., Gorner, H., and Gartner, W. (2011) Peptide release upon photoconversion of 2-nitrobenzyl compounds into nitroso derivatives. *Photochem. Photobiol. 87*, 1031−1035.
(56) Neubauer, C., Gao, Y. G., Andersen, K. R., Dunham, C. M., Kelley, A. C., Hentschel, J., Gerdes, K., Ramakrishnan, V., and Brodersen, D. E. (2009) The structural basis for mRNA recognition and cleavage by the ribosome-dependent endonuclease RelE. *Cell 139*, 1084−1095.
(57) Bahassi, E. M., Salmon, M. A., Van Melderen, L., Bernard, P., and Couturier, M. (1995) F plasmid CcdB killer protein: *ccdB* gene mutants coding for non-cytotoxic proteins which retain their regulatory functions. *Mol. Microbiol. 15*, 1031−1037.
(58) Loris, R., Dao-Thi, M. H., Bahassi, E. M., Van Melderen, L., Poortmans, F., Liddington, R., Couturier, M., and Wyns, L. (1999) Crystal structure of CcdB, a topoisomerase poison from *E. coli*. *J. Mol. Biol. 285*, 1667−1677.
(59) Magnuson, R., and Yarmolinsky, M. B. (1998) Corepression of the P1 addiction operon by Phd and Doc. *J. Bacteriol. 180*, 6342−6351.
(60) Mattison, K., Wilbur, J. S., So, M., and Brennan, R. G. (2006) Structure of FitAB from *Neisseria gonorrhoeae* bound to DNA reveals a tetramer of toxin-antitoxin heterodimers containing pin domains and ribbon-helix-helix motifs. *J. Biol. Chem. 281*, 37942−37951.
(61) Hurley, J. M., and Woychik, N. A. (2009) Bacterial toxin HigB associates with ribosomes and mediates translation-dependent mRNA cleavage at A-rich sites. *J. Biol. Chem. 284*, 18605−18613.
(62) Korch, S. B., and Hill, T. M. (2006) Ectopic overexpression of wild-type and mutant *hipA* genes in *Escherichia coli*: Effects on macromolecular synthesis and persister formation. *J. Bacteriol. 188*, 3826−3836.
(63) Kamphuis, M. B., Bonvin, A. M., Monti, M. C., Lemonnier, M., Munoz-Gomez, A., van den Heuvel, R. H., Diaz-Orejas, R., and Boelens, R. (2006) Model for RNA binding and the catalytic site of the RNase Kid of the bacterial *parD* toxin-antitoxin system. *J. Mol. Biol. 357*, 115−126.
(64) Li, G. Y., Zhang, Y., Chan, M. C., Mal, T. K., Hoeflich, K. P., Inouye, M., and Ikura, M. (2006) Characterization of dual substrate binding sites in the homodimeric structure of *Escherichia coli* mRNA interferase MazF. *J. Mol. Biol. 357*, 139−150.
(65) Brown, B. L., Grigoriu, S., Kim, Y., Arruda, J. M., Davenport, A., Wood, T. K., Peti, W., and Page, R. (2009) Three dimensional structure of the MqsR:MqsA complex: A novel TA pair comprised of a toxin homologous to RelE and an antitoxin with unique properties. *PLoS Pathog. 5*, e1000706.
(66) Agarwal, S., Mishra, N. K., Bhatnagar, S., and Bhatnagar, R. (2010) PemK toxin of *Bacillus anthracis* is a ribonuclease: An insight into its active site, structure, and function. *J. Biol. Chem. 285*, 7254−7270.
(67) Khoo, S. K., Loll, B., Chan, W. T., Shoeman, R. L., Ngoo, L., Yeo, C. C., and Meinhart, A. (2007) Molecular and structural characterization of the PezAT chromosomal toxin-antitoxin system of the human pathogen *Streptococcus pneumoniae*. *J. Biol. Chem. 282*, 19606−19618.
(68) Sedwick, C. (2011) PezT: A bacterial suicide gene. *PLoS Biol. 9*, e1001036.
(69) Min, A. B., Miallau, L., Sawaya, M. R., Habel, J., Cascio, D., and Eisenberg, D. (2012) The crystal structure of the Rv0301-Rv0300 VapBC-3 toxin-antitoxin complex from *M. tuberculosis* reveals a Mg^{2+} ion in the active site and a putative RNA-binding site. *Protein Sci. 21*, 1754−1767.
(70) Miallau, L., Faller, M., Chiang, J., Arbing, M., Guo, F., Cascio, D., and Eisenberg, D. (2009) Structure and proposed activity of a member of the VapBC family of toxin-antitoxin systems. VapBC-5 from *Mycobacterium tuberculosis*. *J. Biol. Chem. 284*, 276−283.
(71) Dienemann, C., Boggild, A., Winther, K. S., Gerdes, K., and Brodersen, D. E. (2011) Crystal structure of the VapBC toxin-antitoxin complex from *Shigella flexneri* reveals a hetero-octameric DNA-binding assembly. *J. Mol. Biol. 414*, 713−722.
(72) Armalyte, J., Jurenaite, M., Beinoraviciute, G., Teiserskas, J., and Suziedeliene, E. (2012) Characterization of *Escherichia coli dinJ-yafQ* toxin-antitoxin system using insights from mutagenesis data. *J. Bacteriol. 194*, 1523−1532.
(73) Meinhart, A., Alonso, J. C., Strater, N., and Saenger, W. (2003) Crystal structure of the plasmid maintenance system ε/ζ: Functional mechanism of toxin ζ and inactivation by $\varepsilon_2\zeta_2$ complex formation. *Proc. Natl. Acad. Sci. U.S.A. 100*, 1661−1666.
(74) Crooks, G. E., Hon, G., Chandonia, J. M., and Brenner, S. E. (2004) WebLogo: A sequence logo generator. *Genome Res. 14*, 1188−1190.